ADVANCED MATERIALS
www.advmat.de

Recent Progress in Solid-State Nanopores

*Kidan Lee, Kyeong-Beom Park, Hyung-Jun Kim, Jae-Seok Yu, Hongsik Chae, Hyun-Mi Kim, and Ki-Bum Kim**

The solid-state nanopore has attracted much attention as a next-generation DNA sequencing tool or a single-molecule biosensor platform with its high sensitivity of biomolecule detection. The platform has advantages of processability, robustness of the device, and flexibility in the nanopore dimensions as compared with the protein nanopore, but with the limitation of insufficient spatial and temporal resolution to be utilized in DNA sequencing. Here, the fundamental principles of the solid-state nanopore are summarized to illustrate the novelty of the device, and improvements in the performance of the platform in terms of device fabrication are explained. The efforts to reduce the electrical noise of solid-state nanopore devices, and thus to enhance the sensitivity of detection, are presented along with detailed descriptions of the noise properties of the solid-state nanopore. Applications of 2D materials including graphene, h-BN, and MoS_2 as a nanopore membrane to enhance the spatial resolution of nanopore detection, and organic coatings on the nanopore membranes for the addition of chemical functionality to the nanopore are summarized. Finally, the recently reported applications of the solid-state nanopore are categorized and described according to the target biomolecules: DNA-bound proteins, modified DNA structures, proteins, and protein oligomers.

1. Introduction

The nanopore is a class of a biosensor, allowing for highly sensitive detection of biomolecules including nucleic acids and proteins at single-molecule resolution.[1–3] The high sensitivity of the nanopore facilitates detection of biomolecules at low concentration even at a sub-nanomolar level and discrimination of minute differences in molecular structure between different nucleotides.[4–6] Such sensitivity originates from the characteristic structure of the nanopore: a nanometer scale pore as large as the size of the target molecule.[7,8] An electric potential applied across the nanopore membrane generates a highly concentrated electric field near the nanopore, driving charged molecules to pass through the narrow pore one molecule at a time.[9] Among the methods to detect the biomolecule translocation including resistive pulse sensing,[3,10,11] tunneling current detection,[12,13] and optical sensing,[14,15] we focus on the resistive pulse sensing mechanism. In the resistive pulse sensing, the nanopore acts as the only channel across the membrane for both ions and biomolecules, and partial blocking of the nanopore by a biomolecule is directly reflected in a perturbation in the ionic current.

The first nanopore used for nucleic acid sensing in 1996 was α-hemolysin, a naturally occurring protein channel secreted by *Staphylococcus aureus*, embedded in a lipid bilayer.[1] It was demonstrated that single-stranded DNA (ssDNA) was electrophoretically transported through α-hemolysin and generated an ionic current drop during the translocation. The ssDNA translocation was confirmed by polymerase chain reaction (PCR) of the solution on the opposite chamber, followed by gel electrophoresis.[1] Solid-state nanopore was suggested in the early 21st century, which complemented the limitations of the biological nanopore such as its unmodifiable pore size, and mechanical and chemical instability.[2,16,17] Conventional structure of the solid-state nanopore mimics the structure of the biological nanopore: a nanopore a few nanometers in size perforated in a 10–20 nm thick silicon nitride (SiN) freestanding membrane, supported by a silicon (Si) substrate. The solid-state nanopore with adjustable pore size and robustness has broadened the range of the target biomolecules for nanopore-based detection, the structure of the device, and materials used for fabrication. Therefore, ever since its first appearance nearly two decades ago, various fabrication techniques and applications of the solid-state nanopore have been actively studied and discussed by researchers from diverse disciplines such as materials science, biomedical engineering, electrical engineering, biophysics, chemistry, mechanical engineering, and medicine.

There are excellent articles in the literature with a thorough and deep insight into the nanopore field, thus highly advisable to read. Deamer and Branton, cofounders of the field, provided the fundamental understanding and prospects of biomolecule detection using the nanopore.[11,18] Dekker introduced the solid-state nanopore and its operating principles,[2] which were further

K. Lee, K.-B. Park, H.-J. Kim, J.-S. Yu, H. Chae, Prof. K.-B. Kim
Department of Materials Science and Engineering
Seoul National University
Seoul 08826, Republic of Korea
E-mail: kibum@snu.ac.kr
Dr. H.-M. Kim, Prof. K.-B. Kim
Research Institute of Advanced Materials
Seoul National University
Seoul 08826, Republic of Korea
The ORCID identification number(s) for the author(s) of this article can be found under https://doi.org/10.1002/adma.201704680.

DOI: 10.1002/adma.201704680

discussed in detail by Venkatesan and Bashir[12] and Wanunu.[3] Extensive reviews on the applications of the nanopore have been published by various groups including Stoloff and Wanunu[19] and Squires et al.[20] Recently, Li et al. summarized the developments in the solid-state nanopores with a focus on the resolution of the nanopore.[21] To our knowledge, our work is the first review to mainly discuss the improvements in the solid-state nanopore in terms of the device and how the upgraded device performance has been applied to the nanopore-based biomolecule detection. The historical scope of this review covers the recent progress as well as the earlier reports on the solid-state nanopore. Although the topic of this review is the solid-state nanopore, we will begin our discussion from the biological nanopore to explain the historical background of the solid-state nanopore.

Ki-Bum Kim is a Professor in the Department of Materials Science and Engineering at Seoul National University, Republic of Korea. He received his B.S. and M.S. degrees in metallurgical engineering from Seoul National University, and his Ph.D. degree in materials science and engineering from Stanford University. Currently, his research interests include the fabrication of novel nanoscale materials and devices such as graphene, transparent conducting oxide, nanopore, and nanochannel structures for manipulation of ions or biomolecules.

1.1. History of the Solid-State Nanopore

The historical timeline of the advancements in the biological nanopore and the solid-state nanopore is summarized in **Figure 1**, where the numbers in the center column represent the date of each event reported. The concept of nanopore sensing was first visualized in 1989 as a sketch in David Deamer's notebook,[22] and filed as a patent in 1995.[23] The first experimental demonstration of nanopore sensing was introduced in 1996, in the paper published by Kasianowicz et al.[1] The first introduced and tested nanopore was α-hemolysin, which is a protein channel with its pore size large enough (stem diameter ≈2.6 nm, limiting aperture size ≈1.5 nm) for a single strand of DNA to pass through.[1,23–25] In addition to the experimental demonstration, the founders presented their insight of the nanopore as a next-generation DNA sequencing tool and claimed that the platform required several improvements for such practical use. According to their opinion, the nanopore should have sufficient spatial and temporal resolution and mechanical robustness, the DNA should move only in the forward direction inside the nanopore for higher accuracy of detection, and different nucleotides should produce different ionic current signals from the nanopore to be distinguished from one another.[1] These guidelines have been widely accepted by nanopore researchers and have been serving as a norm in all nanopore research since the first publication.

Three years after the first report, Akeson et al. experimentally verified their idea of nucleotide type discrimination using the ionic current signals of polyadenine, polycytosine, and polyuracil translocation through α-hemolysin.[6] As they proposed, different types of nucleotides produced current drop signals of different magnitude and duration during the molecular translocation through the biological nanopore.[4,6,11] Nonetheless, DNA sequencing using the nanopore still required slower DNA translocation to read all the nucleobases at a resolvable speed. In 1999, the translocation speed of ssDNA through α-hemolysin was about 1 nucleotide per microsecond, ≈1000 times faster than the ideal speed of 1 nucleotide per millisecond; the ideal value was determined to the extent that the nanopore DNA sequencing is still fast, but a sufficient amount of an ionic current signal is obtained from single nucleotides.[6,12]

Therefore, at the early stage of the biological nanopore, several engineering approaches were suggested to slow down the DNA translocation speed.[12,26,27] In 2012, state-of-the-art DNA sequencing using the biological nanopore—application of phi29 DNA polymerase to control the translocation speed—was introduced by two groups at the same time.[28–30] The enzyme was bound to a DNA molecule, held the DNA to pass through the nanopore slowly at the first stage of translocation, and promoted DNA polymerization at the second stage. Consequently, the partially translocated DNA moved backward, and the same sequence was read again. The same concept and result were published simultaneously using α-hemolysin[28] and *Mycobacterium smegmatis* porin A (MspA) nanopore[29]; MspA is a type of protein channel, with the narrowest aperture of ≈1 nm diameter and ≈1 nm thickness.[31] Using this strategy, single-nucleotide resolution of the biological nanopore has been achieved in the two studies, and DNA sequencing with up to 90% accuracy was reported.[28,29]

Recently, other than α-hemolysin and MspA, various biological nanopores including *Escherichia coli* cytolysin A (ClyA),[32] bacteriophage phi29 DNA packaging motor,[33] bacteriophage SPP1 DNA packaging motor,[34] and aerolysin[35] were reported. The diameter of the narrowest constriction, representative experimental results, and major characteristics of various protein nanopores and the solid-state nanopore are summarized in **Table 1**. These protein nanopores have channels with dimensions of few to several nanometers wide, enabling translocations of relatively large molecules such as dsDNA, protein, and DNA–protein complexes.

The biological nanopore has shown its high sensitivity and resolution, but it had issues of mechanical and chemical instability, and the target molecules of the biological nanopore were limited by the fixed dimensions of the protein channel.[25] The solid-state nanopore emerged to overcome the limitations of the biological nanopore, being mechanically and chemically robust, size-adjustable, and manufacturable.[16,25] In 2001, the first solid-state nanopore was created in a freestanding SiN membrane on a silicon substrate, by focused ion beam (FIB) etching of the SiN surface to fabricate the pore.[16] The most common form of the solid-state nanopore was first introduced in 2003 by Cees Dekker's group, who first used transmission electron microscopy (TEM) to drill a nanopore having a diameter of a few nanometers.[17]

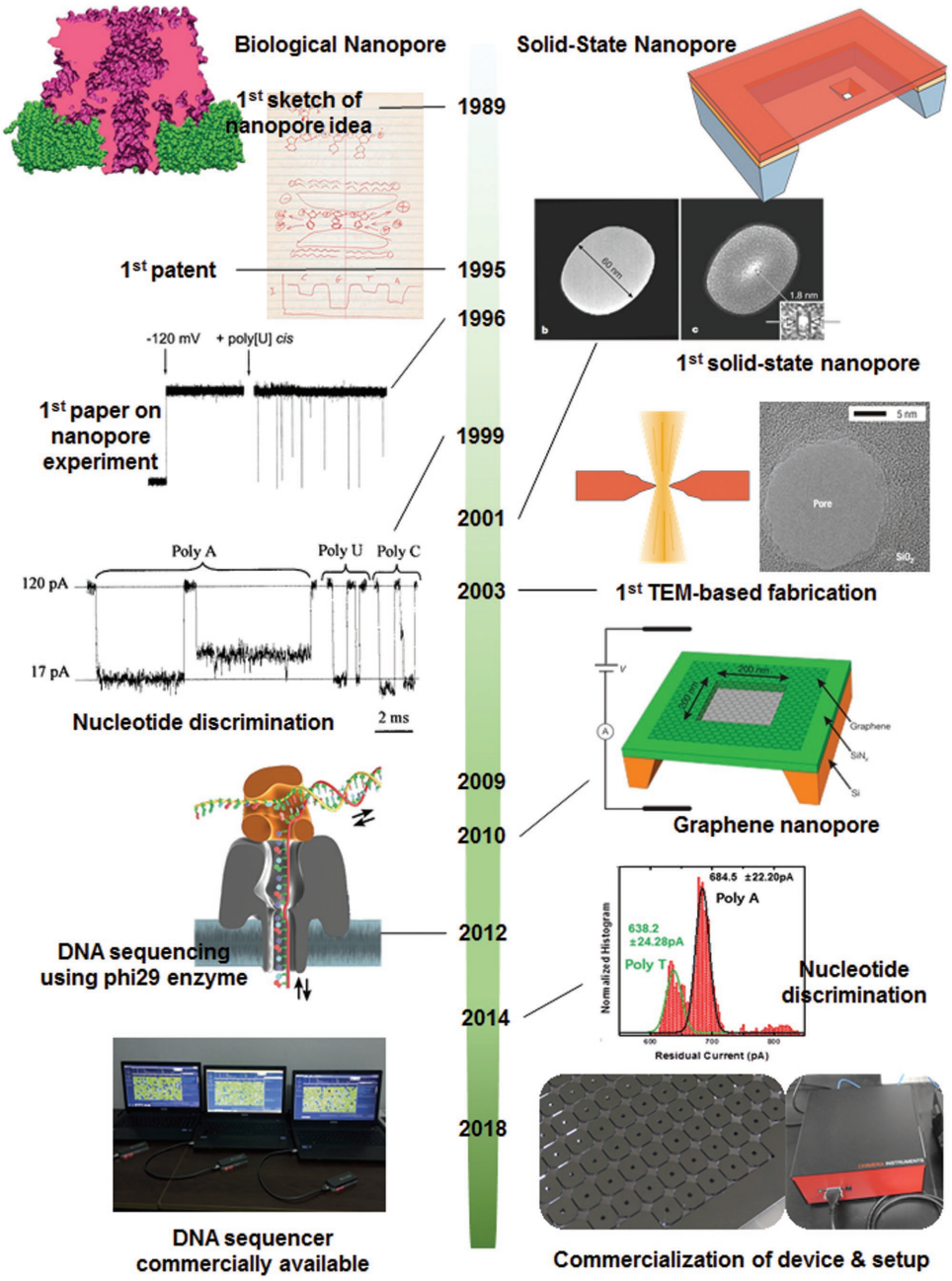

Figure 1. The timeline of developments in the nanopore field: the biological nanopore and the solid-state nanopore. The left and the right columns each show the emergence and the development of the biological (or protein) nanopore and the solid-state nanopore, from top to bottom in chronological order. Atribution of images in the timeline: Biological nanopore column (left): Biological nanopore: Reproduced with permission.[30] Copyright 2012, Nature Publishing Group; first sketch of nanopore idea: Reproduced with permission.[22] Copyright 2016, Nature Publishing Group; first paper on nanopore experiment: Reproduced with permission.[1] Copyright 1996, National Academy of Sciences; Nucleotide discrimination: Reproduced with permission.[6] Copyright 1999, Elsevier; DNA sequencing using phi29 enzyme: Reproduced with permission.[30] Copyright 2012, Nature Publishing Group; DNA squencer commercially available: Reproduced with permission.[82] Copyright 2016, Nature Publishing Group. Solid-state nanopore column (right): Solid-state nanopore: Reproduced with permission.[2] Copyright 2007, Nature Publishing Group; first solid-state nanopore: Reproduced with permission.[16] Copyright 2001, Nature Publishing Group; first TEM-based fabrication (left): Reproduced with permission.[2] Copyright 2007, Nature Publishing Group; first TEM-based fabrication (right): Reproduced with permission.[17] Copyright 2003, Nature Publishing Group; Graphene nanopore: Reproduced with permission.[47] Copyright 2010, Nature Publishing Group; Nucleotide discrimination: Reproduced under the terms of the Creative Commons Attribution License (CC-BY).[8] Copyright 2014, The Authors, published by Nature Publishing Group.

The development of the solid-state nanopore followed that of the biological nanopore with a time interval of nearly a decade. Slowing down the DNA translocation speed has been a major issue also in the solid-state nanopore. Nonetheless, the importance of this issue is greater than that in the biological nanopore because the DNA translocation speed is a few orders of magnitude faster in the solid-state nanopore than in the biological nanopore for an unclear reason.[12] To achieve

Table 1. Summary of the properties of the selected biological nanopores and the solid-state nanopore. The size of the narrowest constriction in each channel, analytes, characteristics, and references are indicated. General characteristics, advantages, and disadvantages of the biological nanopore and the solid-state nanopore are presented as well.

Nanopore		Diameter of narrowest aperture	Representative analytes	Characteristics and remarks		Ref.
Biological nanopore	α-Hemolysin	1.5 nm	ssDNA, RNA, small molecules	First nanopore used in DNA sensing	• Fixed and uniform pore dimensions • Embedded in lipid bilayer membranes • Mechanically vulnerable • Nanopore channels are engineered for specific detection of small molecules or peptides	[1,6,23–25]
	MspA	≈1 nm		Thermally, chemically stable		[27,31]
	Aerolysin	1.0–1.7 nm		Enhanced interaction between DNA and channel wall		[35]
	phi29 packaging motor	3.6 nm	dsDNA, protein	Nonmembrane proteins nor ion channels		[33]
	SPP1 packaging motor	3 nm	Peptide			[34]
	ClyA	3.3–4.2 nm	Protein, protein–peptide complex	Pre-entrance pocket inside the channel		[32]
Solid-state nanopore		Adjustable (minimum ≈1 nm)	ssDNA, dsDNA, protein, DNA–protein and protein–protein complex	• Adjustable but nonuniform pore dimensions • Mechanically and chemically robust • Wide applicability of various materials		[2,17,25]

the slow translocation speed in the solid-state nanopore, various engineering strategies have been attempted: i) modifying the experimental conditions,[36–38] ii) physically dragging the analyte molecule by an optical or magnetic tweezer[39,40] or by electrical gating,[41] and iii) dragging the molecule by strengthened interaction with the modified or chemically decorated pore surface.[42–45] As part of the third strategy, materials including aluminum oxide (Al_2O_3)–graphene,[42] hafnium oxide (HfO_2),[43] zinc oxide (ZnO),[46] organic functionalization,[44] and nanofiber mesh coating[45] were integrated with the nanopores to slow down the DNA translocation by an enhanced Coulombic, specific, or hydrophobic nonspecific interaction between the nanopore surface and DNA.

Along with slowing down the translocation speed, enhancing the vertical and temporal resolution has been one of the major issues in the solid-state nanopore. In 2010, the first reports on the application of graphene membrane to the solid-state nanopore to improve the vertical spatial resolution were published.[47–49] After that, nanopores fabricated in other 2D materials such as hexagonal boron nitride (h-BN)[50–52] and molybdenum disulfide (MoS_2)[53–55] were also reported.

In 2013–2014, nucleotide type discrimination in the solid-state nanopore was first demonstrated.[8,56] The discrimination was possible by fabricating the pore as small and thin as possible (≈1 nm large and ≈5 nm thick) as well as by reducing the electrical noise to enhance the nucleotide resolution of the solid-state nanopore. Particularly, the electrical noise of the solid-state nanopore is an intensively studied subject in this field, and the methods to reduce the electrical noise by applying different materials[8,56–58] or by means of a high-performance data acquisition system[59–61] are well developed.

After the establishment of the high-performance and low-noise system, solid-state nanopore researches mainly have focused on the application of the platform. The applications include detecting DNA single nucleotide polymorphisms (SNPs)[62,63] or DNA methylation,[64] and high-throughput drug screening.[65] These studies are based on the applicability of solid-state nanopore to detection of various biomolecules including double-stranded DNA (dsDNA),[16,66,67] proteins,[7,68,69] DNA–protein complexes,[20,62] and protein–protein complexes.[65,70] Branched from the original solid-state nanopore, glass nanopipettes are also being actively used as cost-effective and high-sensitive solid-state nanopore device.[7,71–77] The solid-state nanopore and the glass nanopipettes each have distinct advantages in terms of fabrication; while the dimensions of the solid-state nanopores can be precisely controlled, the glass nanopipettes are easy and fast to fabricate. Besides the resistive pulse sensing method, optical detection using solid-state nanopores is keep being developed. The latest developments in optical detection using nanopores include electrical–optical synchronized detection using plasmonic nanopore,[78] and integration of nanopore and zero-mode waveguide structure for effective optical DNA sequencing.[79]

Several companies including Oxford Nanopore Technologies, Ionera, Nanopore solutions and Goeppert succeeded in the commercialization of the nanopore DNA sequencing platform or the nanopore device.[80] Oxford Nanopore's MinION sequencer based on the biological nanopores has been applied to genetic sequencing of influenza,[81] Ebola,[82] and Zika viruses.[83] Companies such as Nanopore solutions and Goeppert provide devices and experimental equipment for solid-state nanopore detection. Therefore, the nanopore technology is currently an easily accessible field for DNA sequencing and high-sensitive single-molecular detection of biomolecules.

In summary, for nearly two decades, the solid-state nanopore has been continuously improved in terms of resolution and

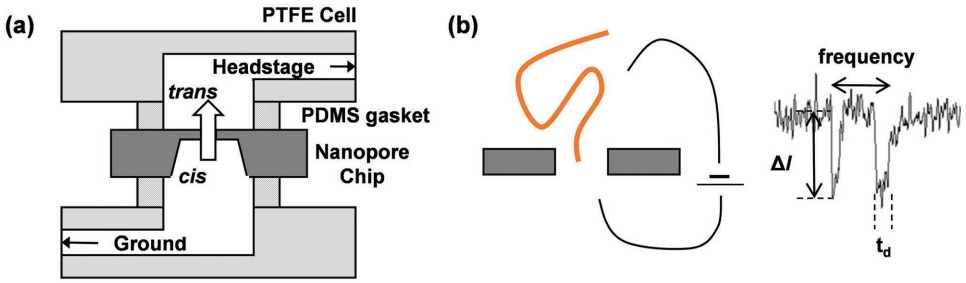

Figure 2. Principles of the solid-state nanopore experiments. a) An example of the experimental settings for solid-state nanopore. The labels indicate each part of the flow cell assembly. Biomolecules move from the *cis* chamber to the *trans* chamber, in the direction indicated by the white arrow. This image is not in scale. b) Diagram of a DNA being electrophoretically translocated (orange coil) through the solid-state nanopore, and resultant ionic current modulation from a real experiment. ΔI, t_d, and event frequency are graphically indicated. This image is not to scale.

sensitivity. The system has also proven its wide applicability to various biomolecules. Herein, we describe the improvements of the solid-state nanopore with a focus on the device and materials used and suggest the outlook of the platform as a multifunctional biomolecule detection instrument.

1.2. Principles of Biomolecule Sensing Using the Solid-State Nanopore

Figure 2 depicts a schematic of the experimental setup and signal production in the solid-state nanopore. As shown in Figure 2a, a nanopore is constructed on a membrane material supported by a substrate, and an electrolyte fills two chambers on both sides of the nanopore. Conventionally, the device is made of Si and SiN as the substrate and the membrane materials respectively, where the Si substrate is anisotropically wet etched to expose the freestanding SiN membrane. The nanopore behaves as the only path for the ions and the biomolecules to translocate between the *cis* and the *trans* chambers.[3] Flow cells are commonly used to create the electrolyte chambers,[57] which are each connected with the ground and headstage electrodes. Guided by the electric potential difference across the membrane, ions and biomolecules move through the nanopore and produce ionic current signals as depicted in Figure 2b.[3,84] A translocating DNA molecule partially blocks the ionic movement through the channel, temporarily reducing the ionic current level. The ionic current recovers to its original level after the translocation.[2,66,85]

The key information among the current-versus-time signals is the drop in current magnitude (blockade current, ΔI), and the duration (dwell time, t_d) and the frequency (capture rate, R_c) of the current drop signal. These results imply the physical information about the biomolecule such as the cross-section area, length, and concentration of the target molecule.[66,67] ΔI reflects the area of the blocked region in the ionic path, thus the size or the cross-section area of the translocated molecule.[7,85] t_d is related to the lateral size of the analyte, and a mechanical force or the interaction between the pore wall and the DNA can also modify t_d.[40,42] R_c expresses how often the DNA is translocated through the nanopore; factors including DNA concentration and the electrophoretic driving force affect the capture rate.[3,9]

Therefore, the fundamental principle of the nanopore-based detection is that biomolecules of different sizes and conformations produce the current drop signals of different magnitude (ΔI) and duration (t_d). This concept has been proven in the experiments using dsDNA of different lengths,[37,66,86] proteins,[7] and different polynucleotides[8,56] or single nucleotides.[53] Nonetheless, the differences in the structures of different nucleotides are very small, such that the nanopore signals of the four nucleotides are difficult to resolve with a solid-state nanopore. The key in the solid-state nanopore is to enhance this resolution; one way to achieve it would be to design and fabricate appropriate devices with such high resolution.

1.3. Fabrication of the Solid-State Nanopore

The device fabrication of the solid-state nanopore consists of two parts: fabricating the freestanding membrane on a supporting substrate and drilling the nanopore.[2,25] The conventional fabrication sequence of the silicon substrate nanopore chip is somewhat standardized using Si substrate and applying semiconductor fabrication technique.[2,17,47,87] To build the nanopore membrane, membrane material—mainly SiN—is deposited onto the substrate, followed by defining and exposing the membrane. Additional or alternative substrate materials used in fabrication include silicon dioxide (SiO_2),[56,59,66] glass,[8,71,72,88,89] and poly(dimethylsiloxane) (PDMS),[58] which mainly act as electrical noise suppressors. In the membrane, oxides such as Al_2O_3 and HfO_2,[42,43,46,90] 2D membranes such as graphene,[42,47,91] h-BN,[50–52] and MoS_2,[53,55,92] and metals[15,93,94] often substitute SiN or are integrated with SiN.

Figure 3 summarizes the representative nanopore perforation procedures. In the pore fabrication technique, FIB appeared as the first method, which works by sputtering the SiN membrane to expose a nanopore on top of the cavity.[16,67,90] Li et al. employed a feedback-controlled system to monitor and control the size of the nanopore with the ion beam.[16] Soon after, TEM nanoporing, the most popular method nowadays, emerged in 2003 with finer resolution and direct imaging mode right after nanopore fabrication (Figure 3a).[2,17] The mechanism of TEM nanoporing was proven as sputtering of the membrane material by electrons from the focused electron beam.[95] With the fineness of the electron beam and better accessibility of TEM than FIB, TEM nanoporing has been accepted as a standard nanopore perforating method.[20] Nonetheless, FIB and TEM nanoporing methods have a fundamental limitation: only a single nanopore can be processed at a time, thus the throughput of fabrication is limited by the poring processes.

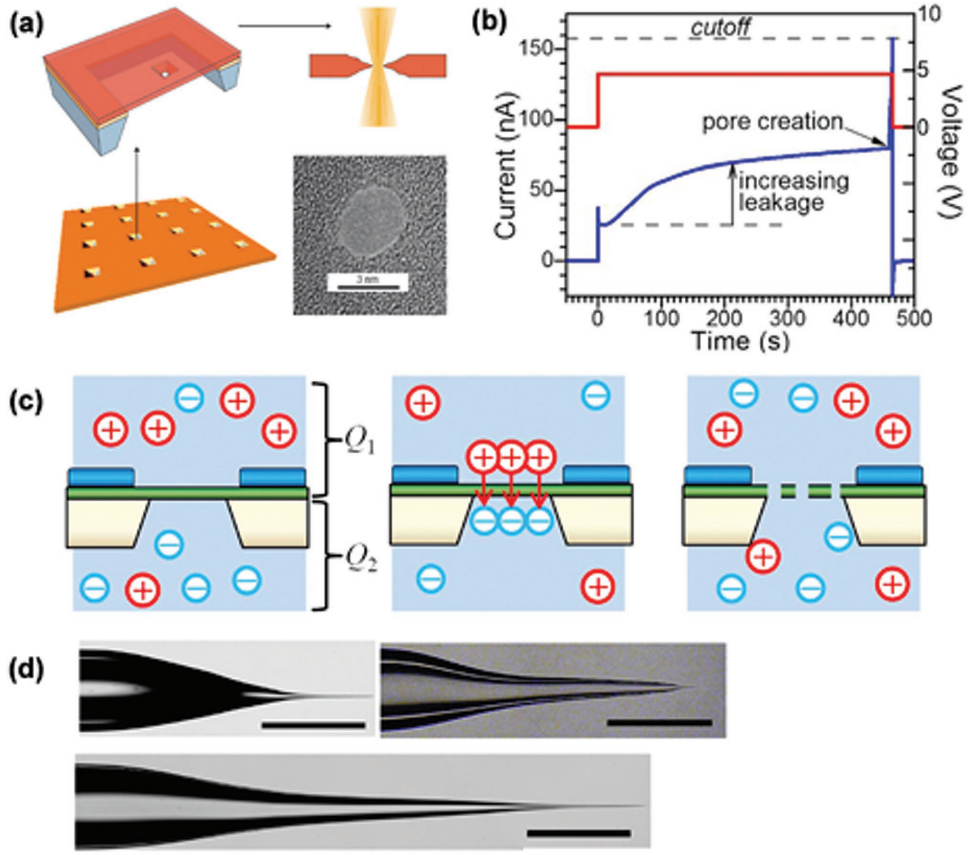

Figure 3. Solid-state nanopore fabrication. a) Schematics of the TEM-based electron beam pore drilling technology. The sample pore diameter is 3 nm. b) Graph of current (blue line) and voltage (red) versus time during the CDB process. c) Mechanism of the controlled dielectric breakdown method for pore formation. d) Images of laser-pulled glass nanocapillaries. The scale bars all indicate 1 mm. a) Reproduced with permission.[2] Copyright 2007, Nature Publishing Group; b) Reproduced under the terms of the under Creative Commons Attribution License (CC-BY).[87] Copyright 2014, The Authors, published by Public Library of Science; c) Reproduced under the terms of the under Creative Commons Attribution License (CC-BY).[97] Copyright 2015, The Authors, published by Nature Publishing Group; d) Reproduced under the terms of the under Creative Commons Attribution License (CC-BY).[89] Copyright 2016, The Authors, published by Public Library of Science.

In 2014, another technique for the formation of a nanopore named controlled dielectric breakdown (CDB) was reported, which uses a strong electric field (on the order of 100 MV m^{-1}) applied across the nanomembrane to mechanically perforate the membrane.[87] In the CDB mechanism, the pore creation is identified in situ by detecting a sudden increase in the ionic current, and the size of the nanopore is controlled at the nanometer scale according to the ionic current level (Figure 3b).[87,93,96,97] Kwok et al. suggested that the mechanism behind the perforation of the nanomembrane is similar to the dielectric breakdown mechanism, in which the name of CDB process is originated (summarized in Figure 3c).[87,97] The biggest advantage of the CDB method is that heavy instruments such as FIB and TEM are unnecessary in this process, lowering the hurdle for fabricating such a small hole at fine resolution. More recently, the CDB process in a SiN membrane less than 10 nm thick was tested, and a voltage pulse was employed for finer control of the size of the ultrathin nanopore.[96]

The nanopores fabricated using TEM or the strong electric field have laterally symmetric structures, namely an hourglass shape[98,99] or a cylindrical structure,[93] respectively. On the contrary, the nanopores perforated using electron beam (e-beam) lithography[94] and laser-pulled glass nanopipettes are in an asymmetric conical shape (Figure 3d).[71,89,100] In general, the dimensions of the narrowest constriction are easily defined and observed using electron microscopes in the symmetric nanopores. In the glass nanocapillary, the effective pore dimensions are estimated from the measured ionic conductance.[74] Nevertheless, the asymmetric pore structure casts noticeable asymmetry of the force field and thus difference in the DNA translocation dynamics in 2 different directions. The geometrical effect on the DNA translocation dynamics was studied based on the advance in DNA manipulation technology, which will be discussed below.[100]

Forming the nanopore is the most important step of the solid-state nanopore fabrication because the sensitivity and reliability of the biomolecule detection are determined by the size and the uniformity of the nanopore structures.[8,56,101] On the other hand, perforating such a small nanopore in a uniform size is a very difficult task, and the throughput of the pore formation is limited in the currently available technologies, especially in the TEM-based method. Therefore, a stable pore fabrication technique should be developed and optimized for mass production of the solid-state nanopore device with uniform structure and device performance.

1.4. Limitations of the Solid-State Nanopore

The solid-state nanopore device and its performance have been continuously improved ever since the first report in 2001, but issues still exist and restrict the platform in terms of the use in actual biological applications.[21] The limitations are mainly resolution and reliability issues: the limit in spatial resolution, both lateral and vertical,[47,102] and in temporal resolution,[12,36,42] and pore clogging during experiment caused by nonspecific adsorption of biomolecules.[103,104]

The limitation in the vertical resolution of a solid-state nanopore originates from the thickness of the membrane. For instance, the conventional SiN membrane of a solid-state nanopore device is about 30–60 times larger than the gap between DNA base pairs of 0.3 nm. Therefore, information of ≈30–60 nucleotides would be read simultaneously, reducing the accuracy of the nanopore detection and the nucleotide resolution. Hence, a thinner membrane is required to enhance the vertical resolution of the solid-state nanopore. The ultimate goal of the thinness would be 0.3 nm, and this thickness value coincides with the thickness of a single layer graphene. Therefore, research interests have naturally focused on fabricating the nanopores with the 2D membrane. As the result, the nanopores fabricated in MoS_2 membranes as well as in thin SiN demonstrated the feasibility of nucleotide discrimination as briefly mentioned above.[8,53,56]

The temporal resolution issue in the solid-state nanopore is caused by excessively fast translocation of the biomolecules across the nanopore. The translocation time of a single molecule is often shorter than the data acquisition interval of the measurement system or comparable to the cutoff frequency of the digital lowpass filter. Therefore, the system often fails to collect data from fast translocation events or distorts the raw ionic current data.[68] Apparently, there are two options for enhancing the temporal resolution of the solid-state nanopore: i) retarding the biomolecule translocation[36] or ii) increasing the data acquisition frequency of the measurement system.[59,61] Nonetheless, expanded bandwidth of data acquisition also collects more electrical noise over the extended frequency range; therefore, enhancing temporal resolution is closely related to the reduction in electrical noise in the solid-state nanopore device.[60]

Apart from the spatial and temporal resolution, the reliability of the solid-state nanopore device should be secured for efficient and stable biomolecule detection. One of the largest barriers for nanopore reliability is nonspecific adsorption of biomolecules onto the membrane or the pore wall.[104,105] These unwanted adsorption patterns produce unpredicted signals,[106] physically block the biomolecules from translocation, and cause temporary or even permanent damage to the device.[103] This issue is being dealt with from the materials perspective, coating of the nanopore membrane with an antifouling material such as poly(ethylene glycol) (PEG) for example.[103,104] The nonspecific adsorption has been studied less than the resolution issues in the nanopore field, so this research category still needs fresh ideas and breakthrough. In addition to the adsorption, mechanical robustness is another issue of the device reliability, particularly when an ultrathin membrane is applied to the device. To reduce the risk of membrane fracture, the free-standing area of the membrane is minimized using e-beam lithography[56] or by inserting an extra supporting layer with a ≈100 nm pore.[51,52,91]

The limitations of the solid-state nanopore discussed above, resolution and reliability, should be resolved to maximize the utility of the biosensing platform. Fundamentally, the nanopore has single-molecular sensitivity, thus its resolution should match such high sensitivity to successfully detect and discriminate biological features. Reliability of the device is generally related to the reliability and the efficiency of the biomolecule detection. In addition, fabricating robust devices may be the foundation of productization and commercialization of the solid-state nanopore platform.

Here, we will discuss how the solid-state nanopore is improved by applying various materials to the substrate and membrane. In Section 2, the improvements of the solid-state nanopore to reduce the noise will be summarized with physical interpretations of the electrical noise in nanopores. Also, reports that aimed at enhancing the spatial resolution of nanopore detection will be discussed. Applying organic materials to the solid-state nanopore membrane is another interesting topic in this field, and we will cover how the organic and biomaterials have provided additional chemical functionalities to the nanopore. In Section 3, we will present the applications of the solid-state nanopore for the detection and characterization of biomolecules. The scope of the nanopore application includes the detection of DNA, structurally modified DNA, DNA–protein complexes, and proteins. Some of the molecules studied are of significance in biology and biomedical applications such as sequence-specific recognition of polynucleotides[62,63,107] and screening of compounds for drug discovery.[65] In the final section, Section 4, we will wrap up our review and suggest the prospects of the solid-state nanopore from the device point of view.

2. Development of the Solid-State Nanopore from the Device Perspective

2.1. Electrical Noise Reduction in the Solid-State Nanopore by Modifying the Substrate Materials

2.1.1. Introduction to Electrical Noise in the Nanopore

In the nanopore detection of biomolecules, the measurement of the ionic currents generates not only the signal but also the electrical noise; thus, the signal-to-noise ratio (SNR) becomes one of the important performance factors of the device. SNR is expressed as $\mathrm{SNR} = \Delta I / I_{\mathrm{RMS}}$, where I_{RMS} is the root-mean-square (RMS or rms) noise of the electrical current flowing through the nanopore under the direct current (DC) bias applied.

Efforts to reduce the RMS noise for higher SNR began with analyzing the noise sources in the nanopore chip and the measurement system. The power spectral density (PSD, S_{I}) curve was obtained from the fast Fourier transform (FFT) of the current trace and was used to analyze the noise characteristics of the nanopore, as presented in **Figure 4**. The noise from the PSD curve is decomposed into four sources each with specific frequency dependences: flicker noise (or $1/f$ noise, indicated as $1/f$ in Figure 4), thermal noise, dielectric noise, and amplifier noise. S_{I} and the frequency dependences of the components of S_{I} are

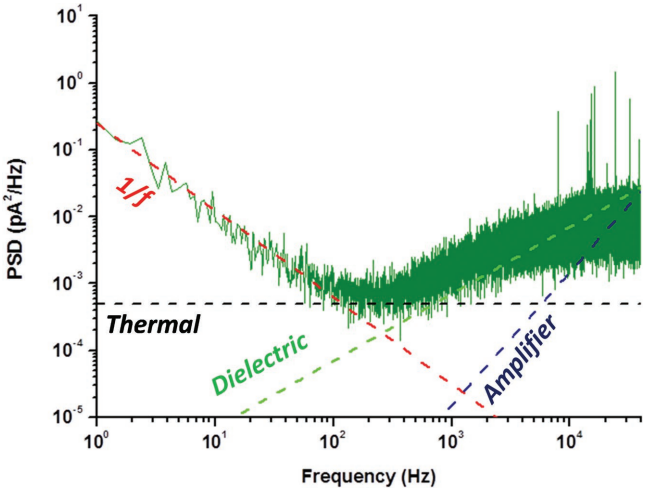

Figure 4. A sample noise power spectrum of a nanopore device. Power spectral density is fitted into a polynomial equation $S(f) = A/f + B + Cf + Df^2$. Each dashed line represents the four noise contributions explained in the text.

expressed in Equation (1), and the integration formula of the PSD curve for I_{RMS} is mathematically described in Equation (2)

$$S_I = S_{Flicker}(\propto 1/f) + S_{Thermal}(\propto 1/R_P) + S_{Dielectric}(\propto f) + S_{Amp}(\propto f^2) \quad (1)$$

$$I_{RMS}^2 = \int S_I df = I_{Flicker}^2(\propto \ln(f)) + I_{Thermal}^2(\propto f/R_P) + I_{Dielectric}^2(\propto f^2) + I_{Amp}^2(\propto f^3) \quad (2)$$

where $S_{Flicker}$, $S_{Thermal}$, $S_{Dielectric}$, and S_{Amp} each indicate the noise powers from each noise sources, f is the frequency, and R_P is the pore resistance.[52,108,109] The frequency range of the integration in Equation (2) is up to the filter cutoff frequency. The I terms on the right side of Equation (2) are the rms noise values from each noise sources.

The four noise components are mainly categorized into two groups, according to the frequency range where each component is dominant. Flicker noise and thermal noise dominate the electrical noise in lower frequency region up to ≈1 kHz.[110,111] Equation (3) (Hooge's relation) and Equation (4) express the noise power spectra of flicker noise and thermal noise, respectively

$$S_{Flicker}/I^2 = A_N/f^\beta = (\alpha/N_C)/f^\beta \quad (3)$$

$$S_{Thermal} = 4kT/R_P = 4kTG_p \quad (4)$$

where I is the ionic current of the nanopore device, A_N is flicker noise power, f is the frequency, α is the Hooge parameter related to the membrane material, N_C is the number of charge carriers in the nanopore, β is a fitting parameter that is generally close to 1.0, k is Boltzmann's constant, T is absolute temperature, and G_p is the nanopore ionic conductance.[110,111] $S_{Flicker}$ and $S_{Thermal}$ are all related to the ionic current level through the nanopore, when $S_{Flicker}$ is also dependent on the membrane material. Because the resistance of the nanopore is quite large due to the small pore size, thermal noise is less pronounced than the other noise sources in typical nanopore measurements.[109]

On the contrary, dielectric and amplifier noises are significantly affected by the properties of the substrate material. Physical descriptions of dielectric noise and amplifier noise are each presented in Equations (5) and (6):

$$S_{Dielectric} = 4kTC_D D_D(2\pi f) \quad (5)$$

$$S_{Amp} \approx (2\pi f(C_D + C_W + C_A)v_n)^2 \quad (6)$$

where C_D and D_D are capacitance and dielectric loss of the nanopore device, C_W and C_A are capacitance terms related to the electrode wiring and the input of the amplifier, respectively, and v_n is the input-referred voltage noise density of the amplifier ($V\ Hz^{-1/2}$).[59,108] Given that the nanopore measurement system consists of an electrochemical circuit, the entire nanopore device can be considered a parallel–plate capacitor.[60,109] The substrate is the major building block of the nanopore chip capacitor in terms of the area and thickness, which means that C_D and D_D are largely determined by the substrate's properties. $S_{Dielectric}$ is the dominant noise source in a wide frequency range of ≈1–100 kHz, so this term has been the primary target for noise reduction in the nanopores. S_{Amp} depends on the performance of the amplifier equipment as well as the nanopore chip. Amplifier noise had not been a big concern because the high-frequency range where amplifier noise acts as the dominant noise source (>100 kHz) was lower than the bandwidths of the lowpass filter typically used in nanopore experiments (10 or 100 kHz). Recently, with the demand for high-frequency measurement even at the MHz level, amplifiers capable of detecting the ionic current at the MHz frequency are being manufactured, thus the importance of suppressing amplifier noise is now increased.[59,61]

2.1.2. Electrical Noise Reduction in the Solid-State Nanopore

Reduction of Flicker (1/f) Noise: Studies aimed at reducing the electrical noise in the solid-state nanopore have been focused on inhibiting each noise source mentioned above. A number of research groups proposed that the low-frequency noise in the solid-state nanopore is attributable to the surface state of the inner nanopore wall such as inhomogeneous surface charge,[112] nanobubble formation,[113] carbon contaminants deposited on the e-beam irradiated site during TEM drilling,[114] or imperfect hydrophilicity of the SiN nanopore surface.[115] Based on these results, modifications of the surface state have been attempted to improve the hydrophilicity and the surface charge homogeneity of the nanopore wall. ALD coating with Al_2O_3 is reported to be effective in decreasing $1/f$ noise,[90] and Tabard-Cossa et al. demonstrated that the nanopore surface treatment with the piranha solution (H_2SO_4:H_2O_2) is effective at reducing flicker noise by ≈two orders of magnitude ($S_{Flicker} \approx 1/f\ (pA^2\ Hz^{-1})$) relative to the bare state ($S_{Flicker} \approx 100/f\ (pA^2\ Hz^{-1})$).[57] Currently, the piranha solution treatments are used by many groups as part of the solid-state nanopore experimental protocol.[56,68,116]

The earlier version of 2D membrane nanopores showed strong flicker noise, ≈two orders of magnitude stronger than

that in the SiN nanopore.[48,117] The suggested origins of strong flicker noise are the hydrophobicity of the 2D materials, the imperfections of the membrane such as pinholes or domain boundaries, and mechanical fluctuation of the thin membrane. When the ionic flow through or near the nanopore hits the membrane, a thinner and larger freestanding membrane is more likely to mechanically fluctuate inside the electrolyte than a thicker and smaller membrane is.[118] In further studies, it was found that using a few layers of the 2D materials instead of a single layer as the nanopore membrane is advantageous for reducing flicker noise.[91,118] In addition, exposing only a small area (>100 nm in diameter) of the membrane to the electrolyte via application of a supporting layer was helpful for improving flicker noise properties in both graphene and h-BN nanopores.[51,119] Combining these methods, the h-BN nanopore with a few layers (6–8 layers) thickness and a small freestanding area (<100 nm diameter) showed improvement in $1/f$ noise level (1–10/f (pA^2 Hz^{-1}) at 100 mV). This low $1/f$ noise level was even comparable to flicker noise of the typical SiN nanopore.[52] Therefore, these results suggested that the mechanical fluctuation of the thin membranes in the electrolyte is one of the major contributors to flicker noise in the 2D membrane nanopores.

Reduction of Dielectric Noise: Dielectric noise and amplifier noise have a significant impact on I_{RMS} because the frequency range where the two sources are dominant occupies a substantial portion of the whole frequency domain. According to Equations (5) and (6), the common factor of dielectric noise and amplifier noise is chip capacitance C_D. Therefore, lowering the chip capacitance is crucial to reduce the total electrical noise of the nanopore device. The efforts to effectively reduce the chip capacitance are categorized into four groups: i) sealing or coating the silicon substrate with polymeric materials,[57,109,120] ii) inserting or depositing a thick dielectric layer underneath the nanopore membrane,[56,59,121] iii) using different substrate materials as a replacement of Si,[8,15,58,88] and iv) using a glass nanopipette or a glass nanocapillary as the nanopore[71,72] (summarized in **Figure 5**). The chip capacitance and dielectric noise power values reported for such modified systems are

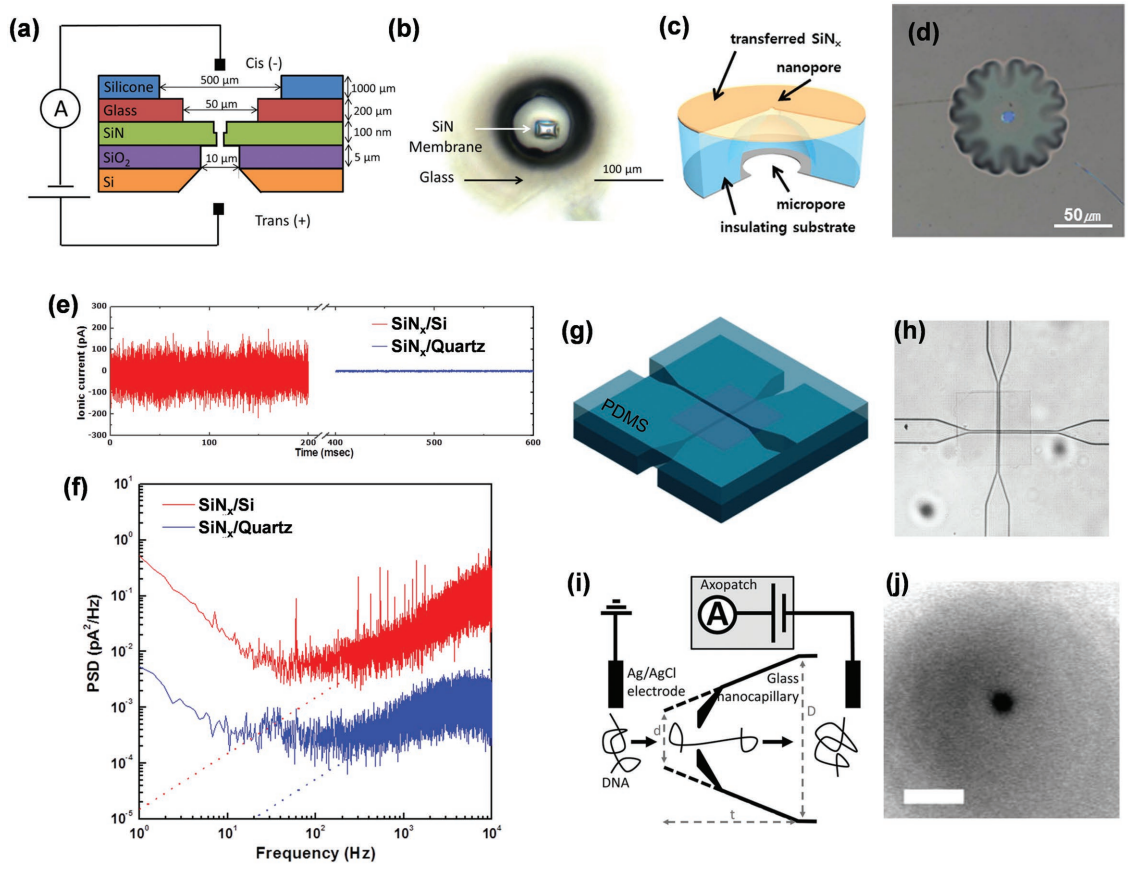

Figure 5. Dielectric noise in the solid-state nanopore. a) Schematic image of the glass bonded nanopore chip. Materials and dimensions are as labeled. b) Optical image of the nanopore chip covered with glass. The scale is as indicated in the lower right corner. c) Schematic image of a quartz substrate nanopore device. d) Optical image of a micropore formed in quartz after transferring the SiN membrane (the blue area at the center). The scale is as inserted. e) Baseline current traces and f) representative noise power spectra of Si (red) and quartz-based devices (blue) measured at 1 M KCl and 0 mV. The dashed lines in (f) indicate the dielectric noise fitting ($S_{Dielectric} \propto f$). g) Schematic image and h) optical microscopy image of microfluidic integrated nanopore devices with PDMS substrates. i) Biomolecule translocation measurement setup of a glass nanocapillary. j) SEM view of a glass nanocapillary after shrinking by means of the electron beam. The scale bar is 50 nm. a,b) Reproduced with permission.[60] Copyright 2014, American Chemical Society; c,d) Reproduced under the terms of the Creative Commons Attribution License (CC-BY).[8] Copyright 2014, The Authors, published by Nature Publishing Group; e,f) Adapted under the terms of the Creative Commons Attribution License (CC-BY).[8] Copyright 2014, The Authors, published by Nature Publishing Group; g,h) Reproduced with permission.[58] Copyright 2013, American Chemical Society; i,j) Reproduced with permission.[71] Copyright 2013, American Chemical Society.

Table 2. Summary of dielectric noise and its reduction methods in the solid-state nanopore. Bare platforms and modified systems are categorized according to the method of the suppression of dielectric noise by reducing the chip capacitance. Short summaries of each method and the reported dielectric noise levels are shown with corresponding references.

Dielectric noise reduction method	Platform	Dielectric noise level ($C \times f$ pA^2 Hz^{-1})	Ref.
Bare platform	α-Hemolysin	$3.5 \times 10^{-8} f$	[57]
	Si/SiN	$3.4 \times 10^{-6} f$	[57]
		$5.3 \times 10^{-5} f$	[111]
Polymeric coating	PDMS-coated	$8.0 \times 10^{-8} f$	[57]
	Imide-coated	$1.6 \times 10^{-7} f$	[109]
	p-PDMS (photodefinable PDMS) coated	$9.6 \times 10^{-8} f$	[120]
Thick dielectric layer deposition	Thick SiO_2 (2.5 μm)-inserted	$1.1 \times 10^{-7} f$	[56]
	Glass-bonded	$4.3 \times 10^{-8} f$	[60]
	Glass-bonded platform + CMOS amplifier integrated	$2.5 \times 10^{-8} f$	[61]
Using dielectric material as the substrate	PDMS substrate	$2.5 \times 10^{-8} f$	[58]
	Quartz substrate	$5.2 \times 10^{-7} f$	[8], Figure 5f
	Pyrex substrate	$3.0 \times 10^{-8} f$	[52]

summarized in **Table 2**. In summary, all the modified devices have manifested a reduction in dielectric noise by 1–2 orders of magnitude in comparison with the conventional Si nanopore.

To seal the exposed membrane, polymers, typically poly(dimethylsiloxane) (PDMS) or polyimide serves as the coating material. After careful coating or patterning of the polymer on the nanopore membrane, the exposed area of the SiN membrane to the electrolyte was reduced to <100 μm in width, reducing the area of SiN that interacts with the ions.[57,109,120] Besides, the polymer sealing method is often used in combination with the thick dielectric layer deposition underneath the nanopore membrane. Materials commonly used for the additional dielectric layer are Al_2O_3 and SiO_2, and the layer is generally prepared by chemical vapor deposition (CVD) or ALD process (Figure 5a,b).[60] The devices with the combination, i.e., Si-substrate nanopore devices with the PDMS coating on top of the SiN membrane and several micrometers thick SiO_2 deposited between the substrate and the SiN layer, are used by several nanopore research groups. The modified devices were reported to have the chip capacitance of ≈50 pF: lower than that of the devices without the dielectric materials applied (≈300 pF), thus leading to low dielectric noise.[43,56,59,68]

Since there is a relatively high dissipation loss between Si and the electrolyte, alternative fabrication methods have been developed to replace the Si substrate with a dielectric substrate. Lee et al. devised a novel solid-state nanopore platform based on a glass substrate (Figure 5c,d) instead of the Si substrate.[8] Figure 5c shows a schematic diagram of a solid-state nanopore fabricated on an insulating quartz substrate, and Figure 5d shows an optical microscope image of the freestanding SiN region on quartz. For fabrication of such device, a two-step wet etching process using hydrofluoric acid (HF) and SiN membrane transfer process were applied to create the amorphous Si (a-Si) supporting membrane with a small SiN opening area (2 μm in diameter). The small SiN freestanding area, as well as the dielectric substrate, lowered the chip capacitance, dielectric noise, and I_{RMS}.[58,60] As shown in Figure 5e, the quartz-based nanopore device showed a low noise level (typical I_{RMS}: 5 pA with a 10 kHz digital filter applied) as compared to the Si-based nanopore device (typical I_{RMS}: 40 pA with a 10 kHz filter). Mathematically, dielectric noise power of the quartz substrate nanopore ($S_{Dielectric,Quartz} = 5.2 \times 10^{-7} f$ (pA^2 Hz^{-1})) was decreased by ≈two orders of magnitude relative to that of the silicon–substrate nanopore ($S_{Dielectric,Si} = 1.5 \times 10^{-5} f$ (pA^2 Hz^{-1})) (Figure 5f).[8]

In a similar concept, the silicon substrate was also substituted by PDMS, a dielectric polymer material. Figure 5g,h shows the schematic image and the optical microscopy image of the microfluidic integrated nanopore device based on the PDMS substrate, respectively. The nanopore membrane of this device was also fabricated by the SiN membrane transfer method and has a minimal opening area of 6 μm^2, which was controllable by adjusting the width of the microfluidic channel.[58] As shown in Table 2, the two devices based on the dielectric substrates (glass or PDMS) showed a similar level of the dielectric noise.

Unlike these substrate-based devices, Figure 5i shows the use of a glass nanopipette as a low-noise solid-state nanopore.[71,89] The glass nanopipettes also showed low device capacitance thus low electrical noise comparable to the glass–substrate nanopore chips.[71,74,89] Although fabrication of the glass nanopipette is relatively easy and fast, the dimensions of the nanopipette are larger (the smallest diameter at the tip is ≈tens of nanometers) and less controllable than the nanopore dimensions are. This relatively blunt probe produces small signals as compared to the small nanopore fabricated by TEM.[71,72,101] To reduce the nanopipette tip size, scanning electron microscope (SEM)-induced shrinking of the nanopipette tip was newly developed (Figure 5j).[71] The shrunk glass nanopipettes had the diameter of 10 nm and demonstrated elaborate tasks such as characterization of DNA–protein complexes and protein–protein interactions.[122,123]

Reduction of Amplifier Noise: The effect of amplifier noise on the nanopore signals and the relation between amplifier noise and the detection frequency is demonstrated in **Figure 6**. In fact, when measured with Axopatch 200B amplifier, which has a maximum filter bandwidth of 100 kHz, a sufficient SNR value above 10 is obtained using a device with the chip capacitance

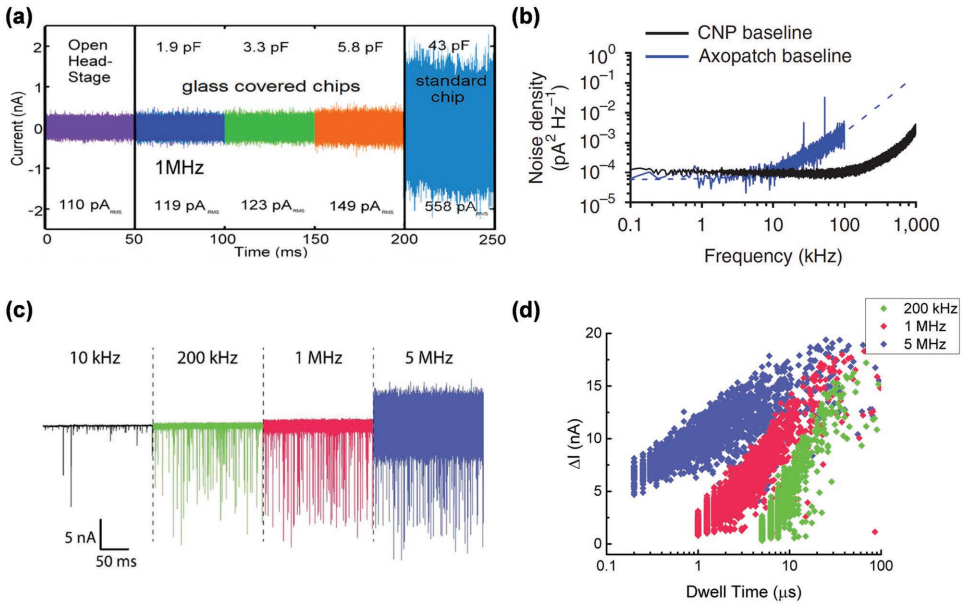

Figure 6. Amplifier noise in the solid-state nanopore. a) Ionic current traces at bandwidth 1 MHz and 0 mV for the open-headstage measurement of several glass-bonded nanopore devices with different chip capacitances, and the standard silicon substrate chip. I_{RMS} values are indicated below each current trace. b) Input-referred baseline current noise spectrum for the CMOS-based preamplifier (black) and an Axopatch 200B in whole-cell mode (dark blue). c) Ionic current traces of 100 nt ssDNA translocation through a nanopore with a 1.3 nm diameter at 900 mV bias under application of lowpass filters with various cutoff frequencies. d) Current blockage versus log-scale dwell time scatter plot for 100 nt ssDNA translocation events in (c). a) Reproduced with permission.[60] Copyright 2014, American Chemical Society; b) Reproduced with permission.[59] Copyright 2012, Nature Publishing Group; c,d) Reproduced with permission.[61] Copyright 2016, American Chemical Society.

of 50 pF.[60] Nevertheless, above 100 kHz bandwidth, amplifier noise becomes the dominant noise source and the signals are often indistinguishable from the noise.

As in dielectric noise reduction, lowering the chip capacitance is also an important contribution to suppressing of amplifier noise. As shown in Figure 6a, the standard chip with 43 pF capacitance yielded a larger rms noise value (558 pA) at 1 MHz bandwidth than that of the glass-covered nanopore chip with 5.8 pF capacitance (149 pA). Even a reduction in C_D by a few pF induced a 30 pA decrease in I_{RMS}, when comparing the glass-covered chips having 5.8 and 1.9 pF C_D.[60] This experimental trend implies that the effect of the chip capacitance on the electrical noise becomes significant at high bandwidths. Based on this result, a two-step fabrication procedure with the insulating glass substrate was developed without the transfer process of SiN membrane, yielding the chip capacitance of <1 pF.[88]

Amplifier noise is also dependent on the performance of the signal amplifier, as presented in Equation (6). In Figure 6b, when the open circuit current was measured without the nanopore chip connected, the complementary metal-oxide-semiconductor (CMOS)-integrated amplifier (CNP) showed a lower high-frequency noise than the ready-made amplifier Axopatch 200B did, owing to the difference in the C_A value (CNP C_A: ≈2 pF, Axopatch 200B C_A: 20 pF).[59] Additionally, when measured with a nanopore with 6 pF C_D, the CMOS amplifiers showed ≈40% lower I_{RMS} than Axopatch ($I_{RMS,CMOS}$: 12.9 pA, $I_{RMS,Axopatch}$: 21.8 pA) at 100 kHz bandwidth.[59]

The low-capacitance amplifier in combination with the low-capacitance chip met the demand for reliable high-frequency biomolecule sensing using the solid-state nanopores. The reported amplifiers include custom-designed amplifiers such as the CMOS-integrated amplifier[59,74,124] and Chimera instruments.[56,60] Figure 6c,d shows an example of the high-frequency detection using the low-noise amplifiers. Figure 6c presents the ionic current trace of 100 nucleotide (nt) long ssDNA translocation events at 900 mV measured by the most advanced CMOS nanopore amplifier (100 ns temporal resolution), with application of lowpass filters at 10 kHz, 200 kHz, 1 MHz, and 5 MHz bandwidth each. Figure 6d is the scatter plot of ΔI versus t_d from the translocation events detected in Figure 6c. As the lowpass filtering frequency increased, baseline noise also increased (Figure 6c), and more information on fast DNA translocation events was obtained (Figure 6d).[61] Therefore, there is a tradeoff between the temporal resolution of the ionic current measurement and I_{RMS} of the system, and it is important to choose an appropriate bandwidth for a high SNR and sufficient data acquisition in each nanopore experiment.

2.2. Improving Resolution and Functionality of the Solid-State Nanopore by Modifying the Membrane Materials

2.2.1. Improving Spatial Resolution of Biomolecules in the Solid-State Nanopore: Applying a Thin Membrane and 2D Materials

To ensure sufficient SNR for DNA sequencing using the solid-state nanopore, a large body of nanopore research has been focused on enhancing the ionic current signal of a DNA translocation as well as on reducing the electrical noise in the nanopore device. Equations (7) and (8) are the mathematical interpretations of the baseline ionic current I_0 and the

magnitude of the blockade current ΔI, assuming that the nanopore is a simple cylindrical resistor with the pore diameter d and the membrane thickness L, at high ionic concentrations (>0.1 M)

$$I_0 = \sigma V\left(\frac{4L}{\pi d^2}+\frac{1}{d}\right)^{-1} \tag{7}$$

and

$$\Delta I = I_0 - \sigma V\left(\frac{4L}{\pi d_{\text{eff}}^2}+\frac{1}{d_{\text{eff}}}\right)^{-1} \tag{8}$$

where σ denotes the ionic conductivity of the electrolyte, V is the applied voltage, d_{eff} is the effective pore diameter when blocked by the DNA expressed as $d_{\text{eff}} = \sqrt{d^2 - d_{\text{DNA}}^2}$, with d_{DNA} as the cross-section area of the linear DNA strand (d_{DNA} = 2.2 nm for dsDNA and d_{DNA} = 1.1 nm for ssDNA).[5,85] According to the above formulae, ΔI would be increased in three ways: i) using the electrolyte with a higher ionic concentration,[36,38] ii) using the nanopore with a smaller pore size,[85,98] and iii) with a thinner membrane.[5,8] Physically, DNA blocks a significant portion of the nanopore when d is small (the difference between d and d_{eff} is larger at small d), enhancing ΔI. Among the three methods, various processes for thinning the membrane have been developed in terms of materials and device fabrication. In addition, thinning the membrane is important for the solid-state nanopore to achieve high vertical resolution of the biomolecules, as previously explained in Section 1.4.

Figure 7 summarizes the structures, fabrication processes, and applications of the solid-state nanopore with a thin membrane for an increased SNR. For instance, Figure 7a illustrates the ionic current traces and corresponding ΔI–t_d scatter plots of 40 nt ssDNA translocation through a 2 nm diameter nanopore in a SiN membrane with thickness variation.[8] Here, to fabricate SiN membranes of different thicknesses, 5–20 nm thick SiN layers were deposited onto the separate substrates and transferred onto the nanopore chip.[8] Consistent with Equation (8), both I_0 and ΔI increased as the membrane thickness decreased, experimentally proving that the membrane thickness should be reduced to obtain large signals from translocating DNA.

Figure 7b presents the process of thinning SiN membrane to thickness <10 nm using e-beam lithography and the resulting atomic force microscopy (AFM) image of the locally thinned SiN membrane.[5] The local thinning process was employed to ensure the mechanical robustness of the etched region. The

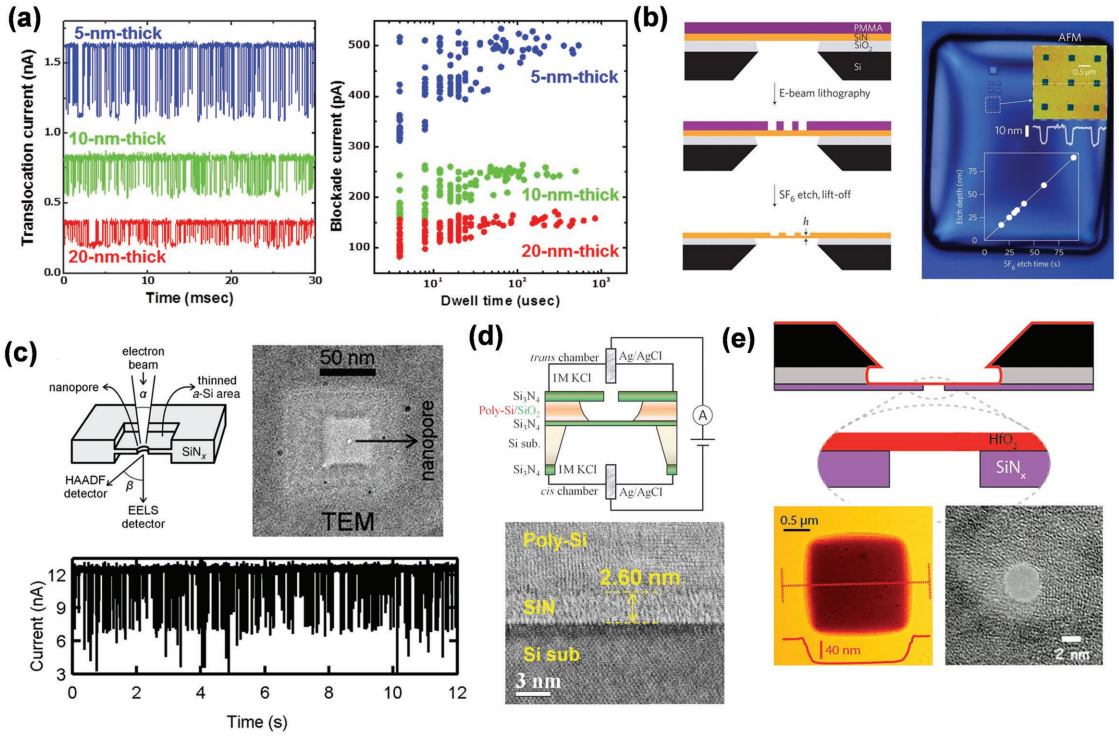

Figure 7. Thin membrane fabrication in the solid-state nanopore. a) Translocation event traces (left) and current-versus-time scatter plot (right) of 40 nt ssDNA passing through a nanopore of different SiN membrane thicknesses. b) SiN membrane thinning process involving e-beam lithography and dry etching processes. The right panel is an optical image of the locally thinned membrane with an atomic force microscopy topographical image of a 3 × 3 array (upper inset) and etch depth-etching time profile (lower inset). c) Schematic of the membrane thinning process using STEM, resulting TEM image, and an ionic current trace of dsDNA translocation through the thin nanopore. d) Device structure of the nanopore device fabricated by the poly-Si sacrificial layer process (top) and scanning tunneling electron microscopy cross-sectional image of 2.6 nm thick SiN membrane and poly-Si sacrificial layer (bottom). e) Structure of the ALD HfO_2 nanopore, and resulting AFM and TEM images of the fabricated HfO_2 nanopore. a) Reproduced under the terms of the under Creative Commons Attribution License (CC-BY).[8] Copyright 2014, The Authors, published by Nature Publishing Group; b) Reproduced with permission.[5] Copyright 2010, Nature Publishing Group; c) Reproduced with permission.[125] Copyright 2015, American Chemical Society; d) Reproduced under the terms of the under Creative Commons Attribution License (CC-BY).[126] Copyright 2015, The Authors, published by Nature Publishing Group; e) Reproduced with permission.[43] Copyright 2013, American Chemical Society.

thinned area had a width in submicron scale and a minimum thickness of 5 nm, which was comparable to the thickness of the lipid bilayer.[56] The thin SiN nanopores showed maximum SNR of 46 when the membrane thickness was 6 nm.[5] Likewise, scanning transmission electron microscope (STEM)-thinning method was employed in SiN nanopore (Figure 7c).[125] This process has an advantage in that the etch process and the poring process can be performed simultaneously by TEM. Here, the area thinned by STEM was ≈63 × 63 nm^2. These nanopores with the local thickness of ≈1 nm provided high blockade conductance ($\Delta G \approx 10$ nS) and high SNR (≈70 at 100 kHz) for dsDNA.[125]

For reduction of the nanopore membrane thickness to less than 5 nm without using e-beam lithography or STEM instruments, a new fabrication process that employed a sacrificial layer of polycrystalline-Si (poly-Si) or SiO_2 (Figure 7d) has been proposed.[126] The role of the sacrificial layer was to restrict the SiN membrane opening area to ≈500 nm wide, providing mechanical robustness to the membrane. As shown in Figure 7d, even a 3 nm thick SiN layer survived the double-etch processes of the Si substrate and the poly-Si layer. It was claimed that the smallest effective thickness was 0.6 nm, comparable to the thickness of the double-layered graphene nanopore. In addition, the devices were used in combination with the CDB nanopore fabrication technique, reproducibly creating a nanopore with diameter <2 nm.[96]

Besides thinning of the SiN film, various efforts applying new materials as alternative ultrathin membranes have been reported. For instance, Al_2O_3[116,127] and HfO_2[43,68,128] films prepared by ALD were introduced as the membrane material. This idea was based on the advantage of the ALD process: continuous film less than a few nm thick can be deposited, and the thickness can be controlled in an atomic scale. Basically, the ALD-prepared oxide films were deposited above or underneath the SiN membrane, followed by selective etching of SiN to leave only a small area of the oxide membrane to be exposed (Figure 7e).[43] As a result, the HfO_2 nanopore is reported to have the minimum thickness of 3 nm.[43,126]

In terms of fabricating the nanometer-thin nanopores, the recent developments in the growth and utilization of the 2D materials, starting from graphene, have attracted huge interest among nanopore researchers. The 2D materials are among the thinnest materials; a single layer of such materials are as thin as the gap between the base pairs of DNA (0.3–0.5 nm).[129] Applications of the 2D materials to the solid-state nanopore, the device structures, and DNA translocation results are presented in **Figure 8**. Three separate groups demonstrated dsDNA translocation through the graphene nanopore in 2010 (Figure 8a).[47–49] As expected, the thin graphene nanopore showed ≈2 times larger ΔI value when compared with the conventional SiN nanopore of similar diameter (Figure 8b).[47,119] Moreover, ΔI was even more enhanced in smaller graphene nanopores as presented in Figure 8b, the trend is consistent with the physical prediction in Equation (8).

Similarly, other 2D materials have been explored to make atomically thin nanopores. As shown in Figure 8c, Liu et al. first introduced h-BN into the nanopore device and demonstrated the enhancement of ΔI as compared with a similarly sized SiN nanopore.[50] The merit of h-BN over graphene was that it was undamaged after UV–ozone treatment unlike graphene, being advantageous in wetting properties and in preventing the pore clogging from the DNA–nanopore surface interaction.[51] Park et al. also reported the low-noise and highly sensitive h-BN nanopore, with a high SNR of ≈50 at 100 kHz filter bandwidth (Figure 8d).[52]

Recently, transition metal dichalcogenides (TMDs) such as molybdenum disulfide (MoS_2)[53–55,92,130] and tungsten disulfide (WS_2)[131] have newly emerged as another class of 2D materials and were tested as the membrane material of a nanopore. In Figure 8e, detection of the dsDNA translocation is demonstrated using the MoS_2 nanopore, showing an enhanced SNR of over 10.[92] Using the MoS_2 nanopore, Feng et al. succeeded in the identification of ssDNA homopolymers (poly-A_{30}, poly-T_{30}, poly-C_{30}, and poly-G_{30}) and even single nucleotides (Figure 8f).[53] A small MoS_2 nanopore (≈2 nm diameter) was used in combination with room temperature ionic liquids to reduce the DNA translocation velocity. Although the device integrated with the ionic liquids showed relatively poor noise properties of ≈90 pA I_{RMS} at 200 mV, this system was effective enough to detect a single nucleotide even at low temporal resolution (a 10 kHz lowpass filter applied). An interesting feature of the single-layer MoS_2 nanopore is that it can be fabricated without TEM, using electrochemical reaction. Here, the concentrated electric field boosted the local surface dissolution of MoS_2, where the surface dissolution can result from the oxidization of MoS_2.[54]

In summary, the solid-state nanopore fabricated in the 2D material is advantageous for obtaining large translocation signals. Combined with the solutions for low electrical noise, these devices showed high SNR compared to the conventional SiN nanopores. However, one of the long-standing problems of the 2D membrane nanopore is the difficulty with developing a wafer scale process because the fabrication of such device involves the membrane transfer process. Moreover, the transfer process causes a low yield of the device by inducing pinholes, cracks, and contamination during the process. Waduge et al. developed a novel transfer-free process to deposit a pinhole-free graphene membrane a few layers thick, freestanding on a prepatterned SiN nanohole.[132] A similar approach in the MoS_2 nanopore has also been proposed by Waduge et al., to directly fabricate a freestanding MoS_2 membrane on the similar prepatterned aperture of SiN (Figure 8g).[55] In contrast to graphene which conventionally requires metallic catalyst in its synthesis, MoS_2 membrane can be directly synthesized via the reaction of molybdenum and sulfur vapors without a catalyst. The nanopore device made of this directly grown MoS_2 membrane was reported to have noise properties comparable to those of the conventional SiN nanopore, owing to the higher mechanical stability of the directly grown membrane compared to the transferred membrane.[55] Therefore, because of the favorable film quality and the wafer scalability of the fabrication, the direct-growth technology for 2D materials is a suitable fabrication strategy for the high-performance solid-state nanopores.

2.2.2. Improving Functionality of the Solid-State Nanopore: Applying Organic Materials onto the Membrane

The high sensitivity of the solid-state nanopore has prompted researchers to integrate additional functionality into the

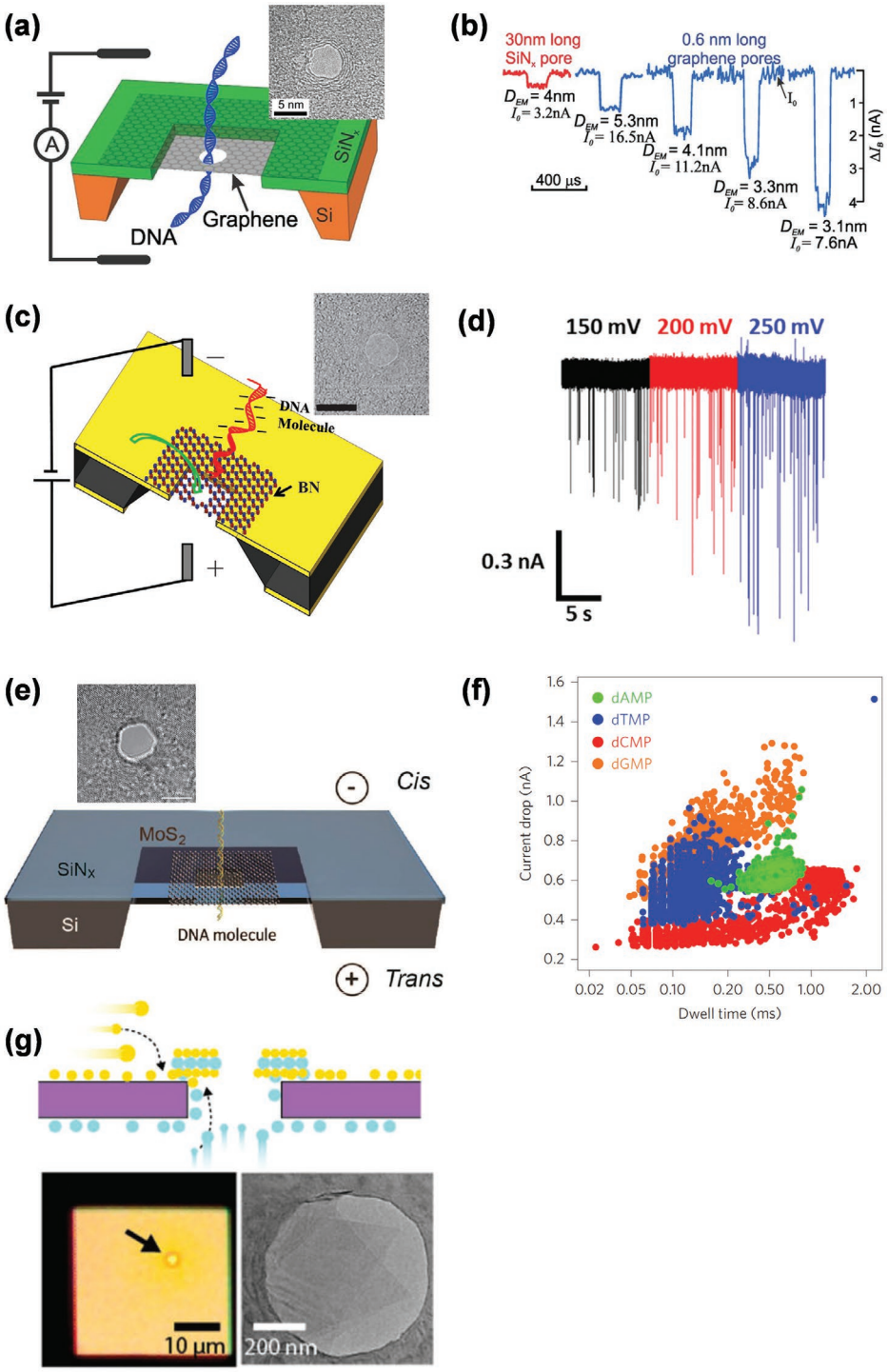

Figure 8. 2D membrane nanopore. a) Schematic structure and a TEM image (inset) of the graphene nanopore device. The scale bar in the inset indicates 5 nm. b) Representative translocation events of dsDNA through the SiN nanopore (red) and the graphene nanopore of different diameters (blue). Scales are as indicated. c) Structure of the nanopore device with a suspended h-BN membrane and a TEM image of an h-BN nanopore (inset). The scale bar in the inset is 10 nm. d) Transport of 1-kbp dsDNA through a multilayered h-BN nanopore with the low-noise glass substrate at different voltages. Scales are indicated at the lower left corner. e) Schematic illustration of a MoS_2 nanopore and DNA translocation through it, and a TEM image of a MoS_2 nanopore with a diameter of ≈5 nm (inset). f) ΔI-t_d Scatter plots of single-nucleotide translocation events through the single-layered MoS_2 pore. g) Schematics of the direct growth mechanism of the MoS_2 membrane and resulting optic and TEM images of the MoS_2 nanopore. a,b) Reproduced with permission.[119] Copyright 2013, The Authors, published by National Academy of Sciences; inset of a) Reproduced with permission.[49] Copyright 2010, American Chemical Society; c) and inset of c) Reproduced with permission.[50] Copyright, Wiley-VCH; d) Reproduced with permission.[52] Copyright 2016, Royal Society of Chemistry; e) Reproduced with permission.[92] Copyright 2014, American Chemical Society; inset of (e), and f) Reproduced with permission.[53] Copyright 2015, Nature Publishing Group; g) Reproduced with permission.[55] Copyright 2015, American Chemical Society.

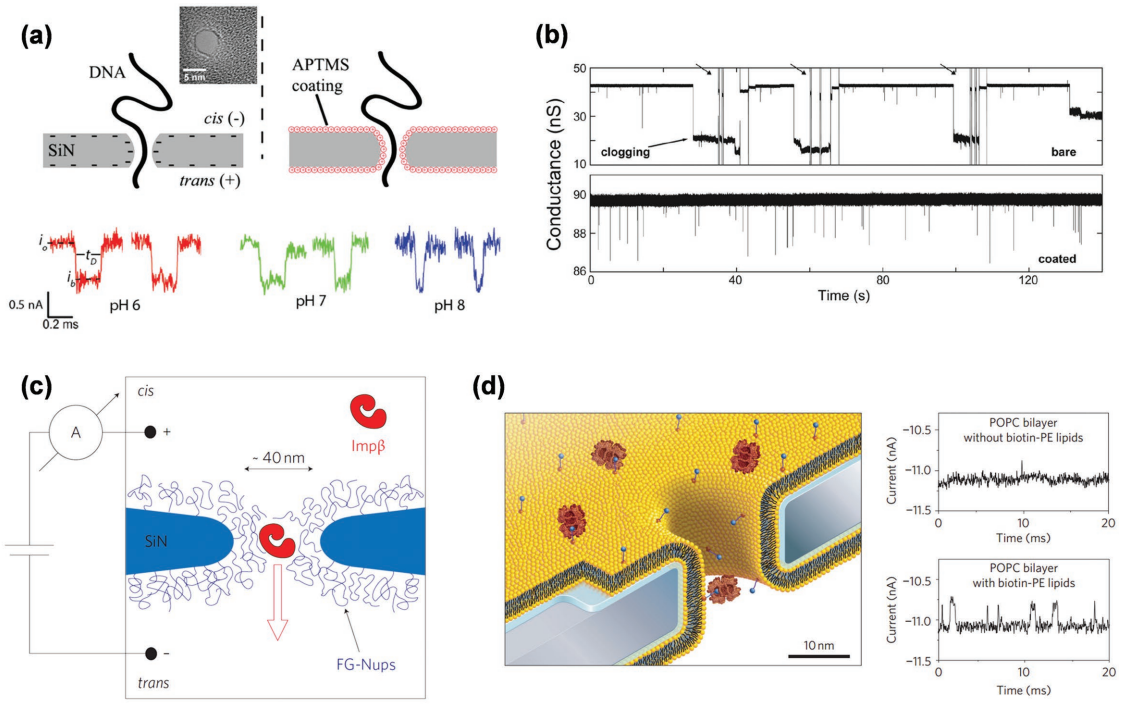

Figure 9. Organic coating on the solid-state nanopore. a) Schematics of the surface charge modification by a 3-aminopropyl trimethoxysilane coating of a nanopore, a TEM image of the surface-modified nanopore and representative DNA translocation events at different electrolyte pHs. b) Current-versus-time traces for ssDNA translocation through the bare nanopore (top) and through a PEG-coated nanopore (bottom). c) A schematic image of the selective Impβ translocation through a Nup-coated nanopore. d) Schematic drawing of streptavidin translocation through a lipid-coated nanopore with a biotinylated anchor (left). The ionic current trace of streptavidin translocation through the nanopores coated with unmodified and modified lipid bilayer (right). a) Reproduced with permission.[133] Copyright 2013, American Chemical Society; b) Reproduced with permission.[104] Copyright 2014, Wiley-VCH; c) Reproduced with permission.[136] Copyright 2011, Nature Publishing Group; d) Reproduced with permission.[135] Copyright 2011, Nature Publishing Group.

platform. This functionality includes controlling the translocation speed of biomolecules,[133–135] preventing nonspecific adsorption of biomolecules on the nanopore surface or clogging,[103,104,135] and enhancing the molecular specificity of detection.[136–138] Organic materials are participants of biochemical interactions, possessing the above functionality acting on biomolecules. Therefore, various organic materials and strategies in biology have been applied to the solid-state nanopore to achieve the advanced functionality. In this section, we introduce the types of organic materials used, the purpose of their application to the solid-state nanopore, how they were prepared, and how they acted. In addition, the concept and the experimental demonstrations of the hybrid nanopore, which is a combination of the biological nanopore and the solid-state nanopore, are discussed.

Application of Organic Coating to the Solid-State Nanopore: Wanunu and Meller first introduced robust procedures for the chemical modification of a SiN nanopore, using a self-assembled monolayer (SAM) of organic molecules.[139] They presented reproducible coating on the nanopores 5–20 nm in size with organosilanes and confirmed the coating by both ex situ analytical method and in situ monitoring of the ion current through the nanopore. This work suggested a framework for the chemical modification of the nanopore surface, and since then, the effects of the organic coating on the biomolecule translocation have been extensively studied.[103,104,133,134,136,137]

Figure 9 presents the representative studies on the application of organic materials to the solid-state nanopore surface. First, organic coatings have been applied to the nanopore to slow down the DNA translocation by enhanced surface–DNA interaction. Anderson et al. modified the surface charge of the nanopore by coating the SiN surface with 3-aminopropyl trimethoxysilane (APTMS), which has a slightly negative charge at pH 8 (Figure 9a).[133] In their experiment, DNA translocation time in the APTMS-coated nanopore was doubled at pH 6 as compared to that at pH 8 (bottom image of Figure 9a), and this was the result of enhanced electrostatic interaction between the positively charged surface and the negatively charged DNA at the low pH. On the contrary, the mean DNA translocation times in the bare SiN nanopore were unchanged at pH 6–8, implying that the surface charge of SiN remained negative in this pH range. In addition, Wang et al. reported that DNA translocation is slowed down in a hydrophilic carboxyl benzyl phosphonic acid-coated SiN nanopore.[134] In combination with a molecular dynamics (MD) simulation, they found that the enhanced interaction based on the hydrogen bonding between DNA and the hydrophilic pore wall is the cause of the slowed down DNA translocation and the increased DNA capture rate.

Besides, self-assembled polymeric coatings on the nanopore surface have been used to prevent pore clogging by biomolecule adsorption on or near the nanopore and to extend the lifetime of the nanopore devices. Tang et al. fabricated a

polyethylene glycol (PEG)-coated SiN nanopore device and reported the reduced adsorption of DNA onto the nanopore surface (Figure 9b).[104] PEG, a representative polymeric antifouling material, was self-assembled on SiN to set the nanopore wall free from the nonspecific binding of DNA. Schneider et al. demonstrated a noncovalent modification of the surface of a graphene nanopore via self-assembly of pyrene ethylene glycol, a type of PEG molecule.[103] The graphene nanopore generally suffers from severe nonspecific adsorption of DNA and pore clogging, which results from the attractive hydrophobic π–π stacking interactions between the nucleobases and graphene. Pyrene ethylene glycol, like other PEGs, prevents DNA from adsorbing on graphene; therefore, even ssDNA, which is stickier than dsDNA, could be detected by means of the PEG-coated graphene nanopore without severe clogging.

Another group of the materials used for functionalization of the solid-state nanopore is biomolecules, including lipids and peptides. Biomolecules can introduce unique functionality to the solid-state nanopores, the most notable of which is selectivity of transport. A summary of the lipid- or peptide-coated solid-state nanopores and their performances is provided in Figure 9c,d. Kowalczyk et al. demonstrated selective transport of biomolecules across a nanopore coated with nucleoporin proteins Nup98 or Nup153 which act as protein transport regulators in the cell nucleus (Figure 9c).[136] The Nup coating on the nanopore acted as a barrier that allowed the passage of only importin-β(Impβ), a protein participating in the transport of other proteins into the cell nucleus, via specific interaction. On the contrary, the translocations of other (nonspecific) proteins (bovine serum albumin in this work) through the same nanopore were restricted in the Impβ decorated nanopore.

Yusko et al. coated the solid-state nanopore with a lipid bilayer to control the pore size and protein translocation through the nanopore (Figure 9d).[135] The lipid bilayer coating was prepared by spreading a unilamellar liposome solution onto the SiN membrane, with biotinylated lipids added to further modify the surface functionality of the nanopore wall. The biotin functional groups attached to the lipid bilayer slowed the translocation speed of streptavidin to a degree sufficient to resolve the translocation signals. Additionally, in the streptavidin-friendly nanopore, the event frequency of streptavidin translocation was higher as compared to those of other proteins that have lower affinities for biotin (antibiotin Fab fragments and antibiotin immunoglobulin G (IgG) antibodies). The lipid coatings were also effective in protecting the nanopore from clogging, by eliminating the nonspecific binding sites for proteins on the nanopore wall. Using this nanopore, amyloid-β (Aβ) oligomer and fibril translocations were detected, whereas the molecules were undetectable due to severe pore clogging in the uncoated pores.[140]

In summary, coating organic materials is an intuitive and effective method for application of chemical functionality to the solid-state nanopore. Using the functionalized solid-state nanopore, it is possible to control and optimize the translocation of target molecules in terms of translocation speed, capture rate, and to eliminate undesired interactions of biomolecules with the pore wall. This biologically inspired strategy is valid in the solid-state nanopore because its target is a wide variety of biomolecules and the origin of the platform itself is the biological nanopore existing in nature. Nevertheless, precise control of the dimensions of the functionalized nanopore is an unresolved issue in this topic because the thickness of the organic coating is less controllable compared to that of inorganic materials subjected to the vapor deposition method.

Hybrid Nanopore: A Combination of the Biological Nanopore and the Solid-State Nanopore: Along with the integration of the solid-state nanopore and the organic coatings, hybridization of the solid-state and the biological nanopores is another branch of application of organic molecules to the solid-state nanopore. The advantages of each component of the hybridized nanopore directly match the limitations of their counterpart: uniform structures, high sensitivity, and the potential for genetic engineering are the merits of the biological nanopore, while it lacks the membrane stability and controllability of the pore dimensions, which are the advantages of the solid-state nanopore.[141] Therefore, the hybrid nanopore is expected to possess all the benefits of the solid-state and the biological nanopores.

The schematic diagrams of the hybridized nanopores and the ionic current traces produced in such nanopores are shown in **Figure 10**. Hall et al. fabricated the hybrid nanopore by inserting an α-hemolysin nanopore into a solid-state nanopore fabricated in a SiN membrane.[142] Here, to electrophoretically insert α-hemolysin into the SiN nanopore, a 3 kilobase pair (kbp) dsDNA molecule was tethered to α-hemolysin via a 12 nt oligomer at the end of the protein channel. The ionic current traces corresponding to each stage of the α-hemolysin docking are displayed in Figure 10a. Before injection of the tethered α-hemolysin, simple dsDNA translocation through the solid-state nanopore appeared (I). The intermediate step indicated preinsertion (II), followed by formation of the hybrid nanopore represented by a stable and low ionic current level (III). Translocation of ssDNA (not shown) suggested that the hybrid nanopore stayed intact during the measurement and produced similar translocation signals to the typical results from α-hemolysin pores embedded in a lipid bilayer. Yet, the hybrid nanopore is still a challenging field because the imperfect insertion of α-hemolysin into a SiN nanopore is considered a leakage current source, which increases the electrical noise.

The biological nanopore provides structural uniformity of the nanopores, but the fixed dimensions of the channels limit the range of the analyte biomolecules. The newly developed DNA origami technology allows for designing and precisely fabricating a hybridized nanopore with a desired structure and dimension. In DNA origami technology ssDNA designed as a scaffold is employed to create the programmed structure by folding and binding according to the nucleotide sequence.[141] The designed DNA origami nanostructures were first integrated with a solid-state nanopore by Bell et al. (Figure 10b).[143] Similar to the biological and the solid-state hybrid nanopore, the electrophoretically driven embedding of a DNA origami nanopore into the solid-state membrane yielded an abrupt current drop. In addition, λ-DNA detection by means of the DNA origami nanopore showed the usefulness of the hybridized nanopore as a single-molecule resistive-pulse sensor.

The DNA origami technique integrated into the solid-state nanopore enabled chemical functionalization of the nanopore by attaching motifs that provided chemical selectivity

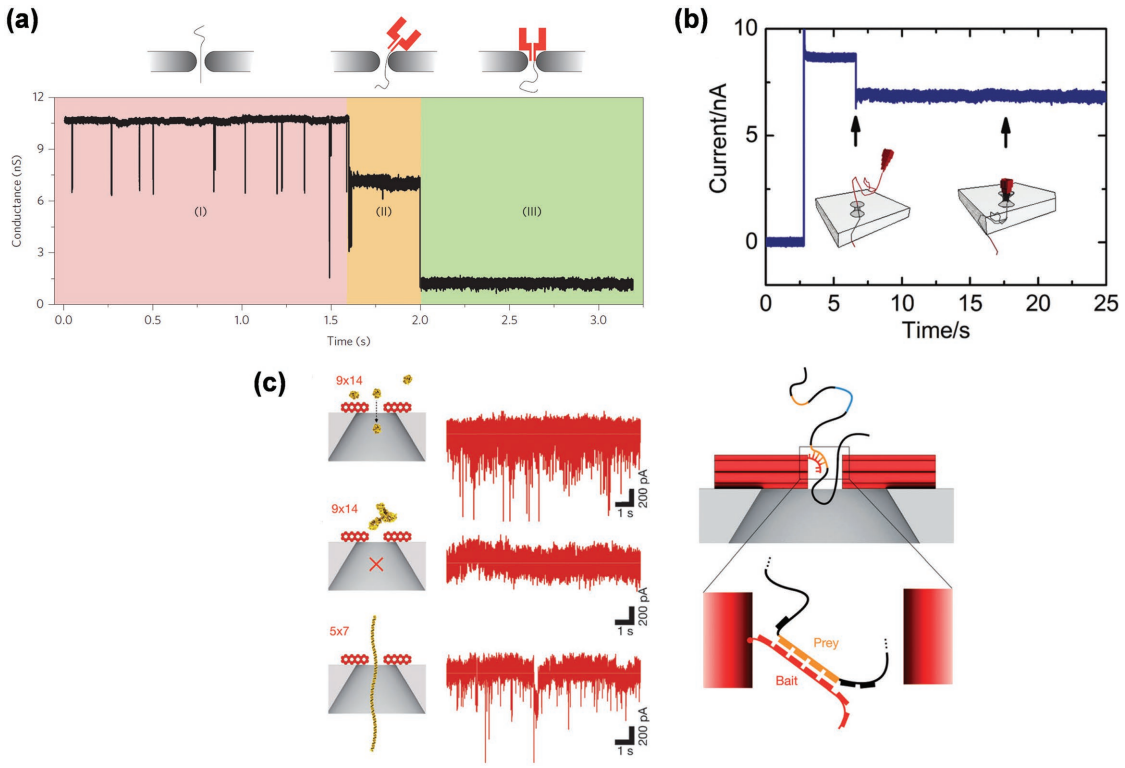

Figure 10. Hybrid nanopore. Current-versus-time traces during the docking of a) an α-hemolysin and b) a DNA origami nanopore into a solid-state nanopore. c) Physical (left) and chemical (right) control of translocation by the DNA origami nanopore. The translocated molecules are streptavidin (left, top), IgG (left, middle), and dsDNA (left, bottom), with the dimensions of the DNA origami nanopores marked in red. a) Reproduced with permission.[142] Copyright 2010, Nature Publishing Group; b) Reproduced with permission.[143] Copyright 2012, American Chemical Society; c) Reproduced with permission.[144] Copyright 2012, Wiley-VCH.

of biomolecule translocation as well as precise control of the nanopore structure. For instance, Wei et al. produced a plateform DNA origami with varying nanopore sizes from 5 to over 10 nm in width, and loaded the self-assembled plates on SiN membrane (Figure 10c).[144] Translocations of various biomolecules (streptavidin, IgG, or dsDNA) were detected by the size-controlled hybridized nanopore (physical control of translocation,[145] left panel of Figure 10c). Also, the protruding ssDNA strand selectively interacted with specific ssDNAs; these interactions translated into exceptionally long-lasting translocation signals (chemical control of translocation,[145] right panel of Figure 10c). Additionally, to understand the structural properties and optimize the experimental conditions of the DNA origami hybridized nanopore, ionic permeability and mechanical stability of the DNA origami were studied at various pore sizes and bias voltages by Plesa et al.[146]

To summarize, the hybrid nanopore is a combination of the top-down and the bottom-up approach of the nanopore device fabrication. The protein nanopore or the DNA origami nanopore brings the uniformity of the nanopore structure to the solid-state nanopore. Conceptually, the idea is feasible and prospective; however, further improvement, i.e., reduction in the ionic current fluctuations from unstable docking is required for a physically or chemically customized and processable nanopore platform with high sensitivity, stability, and versatility.

3. Applications of the Solid-State Nanopore

3.1. Detection of DNA-Bound Proteins and Modified DNA Structures

In addition to the intensive efforts to enhance the performance of the solid-state nanopore devices, various biomolecule detection applications of the solid-state nanopore have also been attempted. In the early years of the solid-state nanopore, the simple linear-form DNA translocation events were mainly studied.[147] With the noticeable advances in the sensitivity of the solid-state nanopore and introduction of DNA modification strategies, the nanopore detection of DNA–protein complexes, DNAs of various structures, and proteins were recently demonstrated. In this section, we introduce the detection of DNA-bound proteins along with DNA–protein complexes and modified DNA structures using the solid-state nanopore.

The detection of the DNA-bound proteins in a DNA–protein complex by means of the solid-state nanopore is summarized in **Figure 11**. When a protein is bound to DNA, the volume of the binding region is bigger than that of bare DNA strands, and this local volume difference results in the additional ionic current drop among the translocation signals. Using this strategy, Kowalczyk et al. successfully detected DNA repair protein RecA's binding to DNA using a SiN nanopore 20 nm thick and 30 nm in diameter (Figure 11a).[148] Detection of dsDNA–RecA

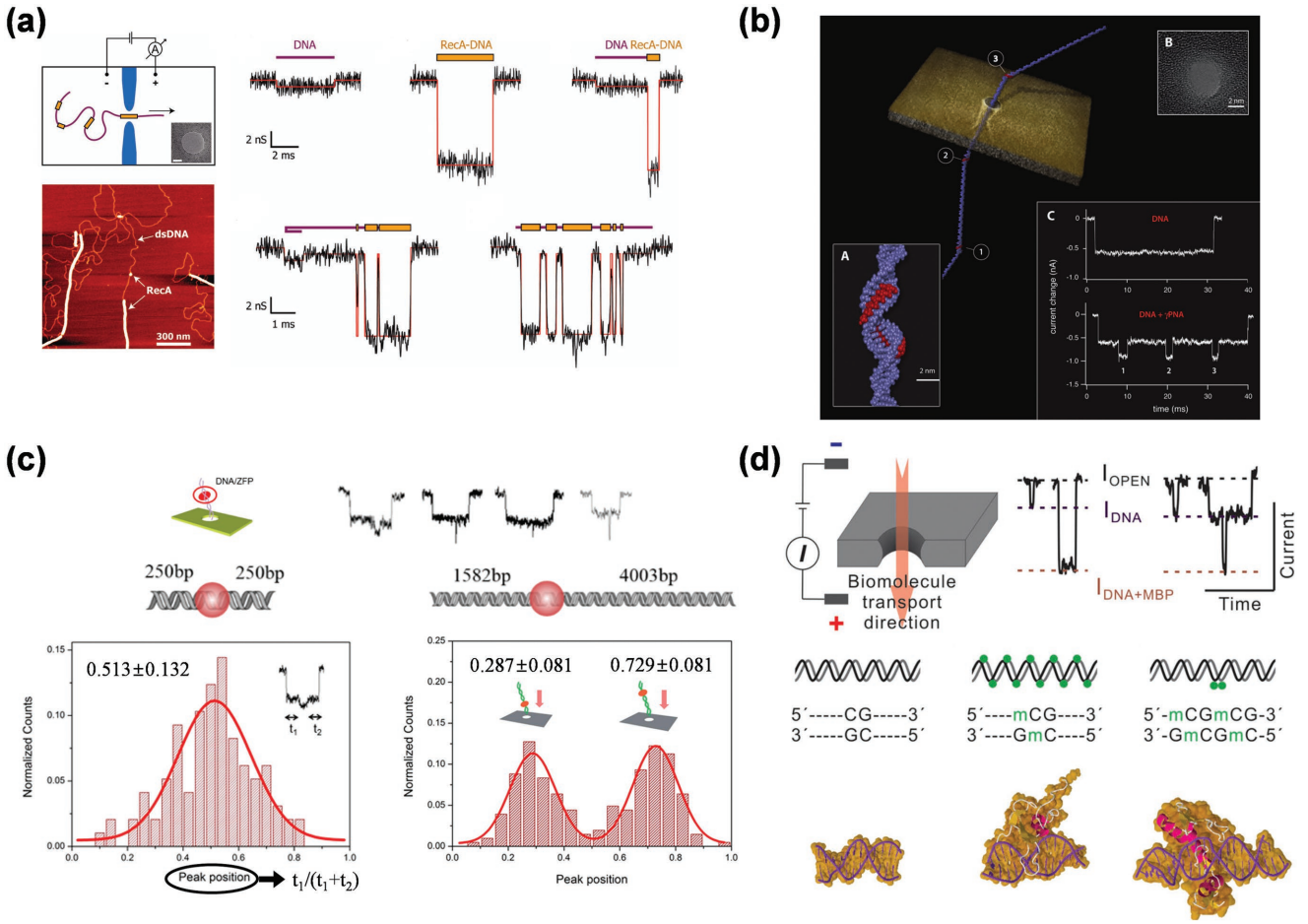

Figure 11. Detection of DNA bound proteins by the solid-state nanopore. a) AFM image of RecA-coated DNA (left) and typical nanopore translocation events of the RecA-coated DNA with the schematic structures of the RecA–DNA complex (right). b) Image and observed translocation signals of PNA-tagged DNA molecules across a solid-state nanopore. c) Representative nanopore events of DNA–ZFP complexes (top) and the relative ZFP-binding positions determined from the positions of the secondary peak inside each translocation signal (bottom). d) Nanopore detection of hypermethylated dsDNA and locally methylated dsDNA complexed with MBP. Images below are 2D and 3D visualizations of the structures of DNA–MBP complexes. a) Reproduced with permission.[148] Copyright 2010, American Chemical Society; b) Reproduced with permission.[150] Copyright 2012, American Chemical Society; c) Adapted with permission.[62] Copyright 2015, American Chemical Society; d) Reproduced with permission.[152] Copyright 2015, American Chemical Society.

binding using the solid-state nanopore was previously reported by the same group (not shown in the figure), but they compared only the signals from the bare DNA and the DNA strands wholly covered with RecA in their previous work.[149] As presented in the figure, the nanopore translocation events of RecA–dsDNA complexes resulted in signals having both a low blockade level (bare DNA region, diameter ≈2 nm, $\Delta G < 2$ nS) and a high blockade level (RecA-bound region of DNA, diameter ≈7 nm, $\Delta G > 10$ nS).[148] While a locally coated RecA–DNA complex passed through the nanopore, the location of the perturbation in the ionic current signals directly reflected the location of the bound protein. Considering the measurement bandwidth and the total DNA translocation time, they suggested that 8 nm or 15 base pair spatial resolution of the local protein binding along DNA can be identified at an applied voltage of 10–15 mV.[148]

In the same principle, the attention of the nanopore researchers shifted to detecting sequence-specific binding of proteins or polymers to DNA. This approach is attractive in terms of DNA sequencing: indirect monitoring of the sequence of interest through the binding proteins. Singer et al. studied detection of the complex of dsDNA and peptide nucleic acid (PNA) probe, which is a synthesized polymer binding to specific sequences of DNA (Figure 11b).[150,151] According to the same principle as above, the PNA-bound DNA caused secondary current drops, and relative positions of the target sequences in the DNA strand were determined by reading the intervals between the secondary drops. In addition, they demonstrated that the solid-state nanopore sensors can discriminate the DNAs of two different human immunodeficiency virus (HIV) subtypes by detecting the differences in binding locations of PNA in the two DNA strands.[150]

Subsequently, Yu et al. identified the zinc finger protein (ZFP)-binding position in DNA to a single-protein resolution using a glass-based solid-state nanopore (Figure 11c).[62] As in other studies of the similar principle, the secondary peak represented the local volume change in the ZFP-bound region,

and the relative peak position reflected the location of the ZFP recognition sequences. Two types of ZFP–DNA complexes with different binding locations were distinguishable by the location of the secondary peak. Analysis of the transcription factor ZFP using the solid-state nanopore was also conducted by Squires et al.[63] In that work, translocation events of the ZFP–DNA complexes were categorized into five blockage patterns. Then, the event characteristics such as current drop and dwell time were analyzed to define the identity of each blockage pattern. In addition, they demonstrated that the solid-state nanopore sensors were capable of detecting and discriminating specific and nonspecific modes of ZFP–DNA binding by matching the information from the signal patterns to the known geometry of the DNA–protein complex.

Another specific application of DNA-bound protein sensing using the solid-state nanopore studied by Shim et al. is the detection of DNA methylation, which is potentially related to cancer diagnosis (Figure 11d).[64,152] Hypermethylated 90 bp DNA formed a bulkier complex with methyl-binding proteins (MBPs) compared to unmethylated 90 bp DNA. Therefore, translocation of the DNA–MBP complex produced signals with a ≈6-fold larger current drop and ≈20-fold longer dwell time in comparison with the unmethylated DNA. In addition, 90 bp DNA with a local methylation site at its center was detected using the Kaiso zinc finger (KZF) protein. The secondary current level generated by the bound protein (≈2 nA for the DNA-only region, ≈4 nA for the DNA–protein complex) was clearly detectable and the locations of the sublevel were mostly at the center of each current drop signal. Similarly, nanopore-based detection of anti-DNA antibodies[153] and a single base mismatch in dsDNA using mismatch binding protein MutS[154] and ssDNA binding protein[155] were also studied.

Recently, with the same concept of detecting the local difference in the structure of the translocating molecule, modifications of the DNA structure have been actively studied using the nanopores, expanding the boundaries of solid-state nanopore applications. **Figure 12** summarizes the experimental schemes and brief results of the nanopore research on complex DNA structures. Plesa et al. designed and synthesized DNA containing a protrusion in the main strand, and studied the translocation of such DNA through the solid-state nanopore (Figure 12a).[156] Both the symmetric DNA construct having the protrusion at the central position and the asymmetric DNA construct with the protrusion near the end each showed a characteristic secondary current level among their translocation signals. Furthermore, an increase in the DNA translocation velocity at the end of the translocation process was monitored by analyzing the relative location of the secondary current drop

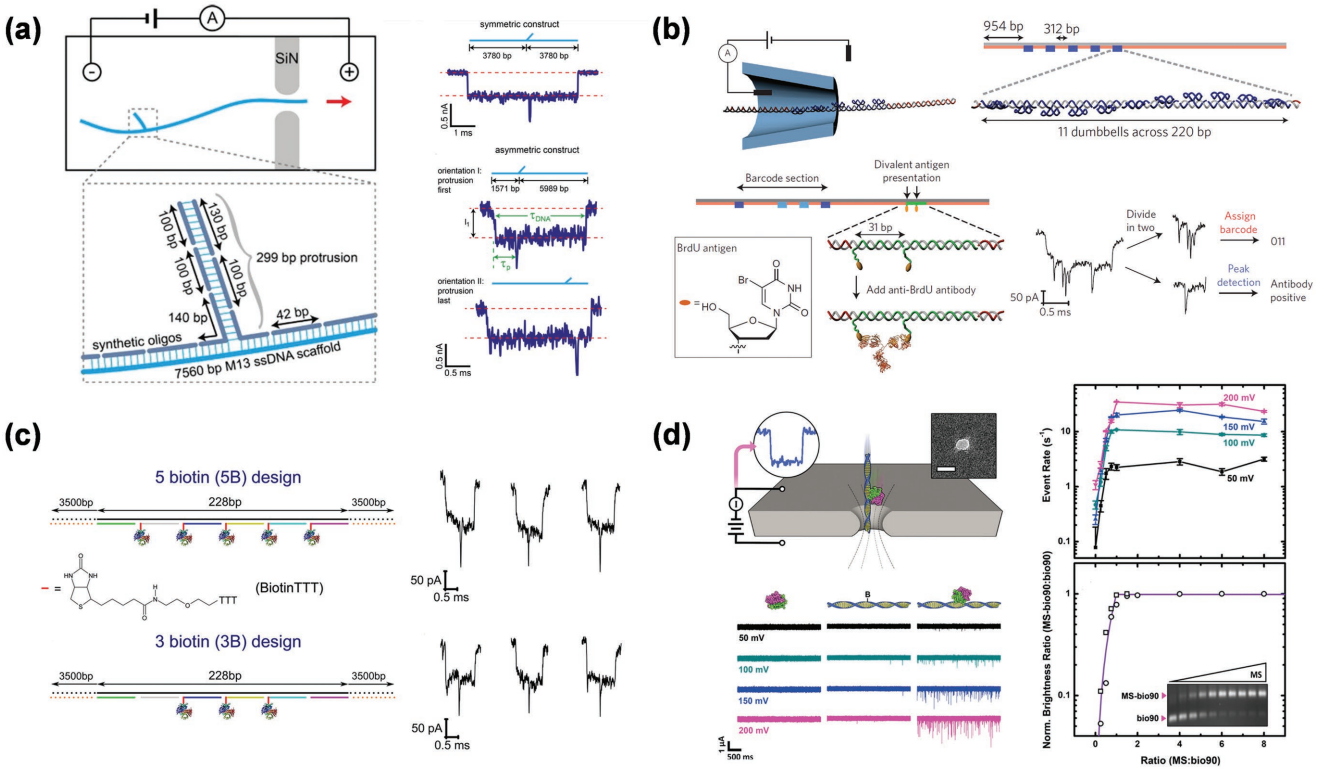

Figure 12. Nanopore detection of modified DNA structures. a) Structure of the modified DNA with a nucleotide branch in the main strand (left) and investigation of the local translocation velocities of DNA using the DNA construct with a protrusion (right). b) Images and nanopore translocation signals of DNA dumbbells designed as a barcode (top) and for the selective detection of antibodies (bottom). c) Structure of engineered dsDNA with multiple biotins and the translocation signals of the biotin-tagged DNA and streptavidin complexes. d) Quantification of biotin-tagged DNA–streptavidin complexes using the solid-state nanopore. The results from the solid-state nanopore and EMSA are presented. a) Reproduced with permission.[156] Copyright 2015, American Chemical Society; b) Reproduced with permission.[76] Copyright 2016, Nature Publishing Group; c) Reproduced under the terms of the under Creative Commons Attribution License (CC-BY).[75] Copyright 2015, American Chemical Society; d) Reproduced with permission.[157] Copyright 2014, American Chemical Society.

in each translocation signal. This is the representative work among the translocation studies of the modified DNA in the solid-state nanopore and shows the use of such DNA structure in the physical analysis of DNA translocation dynamics.

Bell and Keyser modified dsDNA to include a "DNA dumbbell"[76] as the protrusion (Figure 12b). The DNA dumbbells caused characteristic secondary signals similar to those produced by the DNA-binding proteins and other DNA protrusions. Five groups of DNA dumbbells separated by 312 bp from each other produced five discernible secondary current drop signals, acting as a molecular barcode. The reliability of the barcode signals was validated by detecting nanopore translocations of all possible 3 bit codes and discrimination of the eight different signals, which directly reflected the existence and the location of the code. Furthermore, they designed each barcode to carry specific antigens. When mixed with antibodies, the decorated DNA formed DNA–antibody complexes and the binding of four different antibodies were detected simultaneously.[76] The DNA dumbbell was also used to study the dynamics of DNA translocation through the asymmetric glass nanopipette. When translocated from inside the nanopipette to the free solution, DNA was influenced by the tensile force field built inside the nanopipette. Using DNA dumbbells as position markers, Bell et al. found out that the velocity during translocation increased over time, and they validated the observed phenomenon using the optical tweezer experiment and the hydrodynamic model. In the opposite direction, the DNA translocation events were similar to those observed in the symmetric nanopores.[100]

Another novel DNA modification method is "DNA carrier,"[75,77] which is an engineered dsDNA functionalized with a single (or multiple) biotin group(s). Here, the biotin motifs decorated the end of the selected DNA segments, naturally transplanting the biotin site to the engineered DNA carrier upon hybridization. Utilizing the high binding affinity of biotin for streptavidin, Bell and Keyser detected streptavidin binding to DNA within the mixture of four different proteins including streptavidin using the glass capillary nanopore (Figure 12c).[75] Furthermore, with the DNA carrier and the glass capillary nanopore, Kong et al. demonstrated measurement of the binding protein concentration in the ionic solution.[77] As the concentration of streptavidin in the solution increased, the proportion of events having the characteristic streptavidin-biotin current drop also increased. Similarly, the proportion of digoxigenin (dig)-antidigoxigenin (Anti-dig) binding was analyzable using the nanopore. Streptavidin or Anti-dig concentration at a nanomolar level measured by means of a nanopore showed quite good agreement with the electrophoretic mobility shift assay (EMSA) data, which identified the binding fraction by the gel band intensity. These results point to the possibility of solid-state nanopore measurement of nanomolar concentrations of a protein in a microliter level volume.

In addition, several studies have utilized the biotin-tagged DNA to facilitate the nanopore detection of small biomolecules, which are difficult to detect in their bare states. In the study by Carlsen et al., both biotin-tagged short 90 bp DNA and streptavidin were rarely detectable because of too fast translocation and the temporal limitation of the measurement system. On the other hand, the translocation event frequency of the streptavidin-bound DNA–complex increased by more than an order of magnitude than the frequencies of streptavidin or DNA translocations. (Figure 12d).[157] They suggested that the strong electrophoretic driving force acting on streptavidin was partly balanced by the fluid drag exerted on the biotinylated DNA. This resulted in a decrease in the net translocation driving force applied to the DNA–protein complex as compared to each component of the complex, slowing down the translocation speed. Moreover, the relationship between the translocation event frequency of the streptavidin-bound DNA–biotin complex and the concentration of streptavidin was examined using the solid-state nanopore. The result was consistent with the EMSA results, which revealed a similar dependence of the signal intensity on the streptavidin and DNA–biotin concentration ratio. It was also demonstrated that unknown concentrations of DNA–biotin complexes were definable by the translocation event rate.[157]

An advanced approach was tested by Zahid et al., who succeeded in detecting specific target sequences of ssDNA within a heterogeneous mixture of target and nontarget DNAs.[107] The biotin-tagged ssDNA formed dsDNA when ssDNA having the complementary sequence was present in solution, resulting in an increase of the translocation frequency. Using the strategy, they demonstrated detection of hsa-miR-155 (miR155), a biomarker of lung cancer; the biotinylated ssDNA with a sequence complementary to miR155 bound to the target miRNA, and the complex was detected using a solid-state nanopore. Although small biomarkers are generally difficult to detect due to insufficient resolution of the nanopores, the integration of biological engineering into the solid-state nanopore platform facilitates successful and effective detection of such biomolecules.

In summary, the solid-state nanopore has been actively integrated with the state-of-the-art genomic detection of biomarkers. Fundamentally, this approach is the extension of the initial idea of the nanopore application—DNA sequencing. With the advanced genomic design and modification technology, the applications have been more expanded to detecting antigens, small proteins, and miRNAs using DNA complexes and nanopores. These developments have been directed toward detecting smaller features more sensitively or detecting multiple proteins, antigens, or small molecules. Nevertheless, for the elaborated detection in the solid-state nanopores, there still is a need to enhance the reliability of the dwell time measurement because detection of the DNA–protein binding site by means of the solid-state nanopore largely depends on the translocation dwell time. The efforts to improve the temporal reliability of the nanopore detection should include reducing the translocation velocity and the nonspecific interactions between biomolecules and the nanopore wall; the latter induces a large deviation of the dwell time from the translocations of the same biomolecules.[42,43,50] With further improvement of the solid-state nanopore detection sensitivity and reliability of detection, more accurate detection of interesting targets such as DNA–protein complexes and modified DNA structures is expected.

3.2. Detection of Proteins and Protein Oligomers

Although nucleic acids have been at the center of attention over the past decade, proteins are rapidly becoming the prime

target for the solid-state nanopore research.[7,68,158–162] Unlike nucleic acids, each protein has a unique 3D structure and heterogeneous charge profiles. These biophysical properties of protein yield different behaviors from those of nucleic acids, including high pH responsiveness, conformational changes, and specificity in translocation and complexation with other proteins, which are directly reflected in the nanopore signals. In accordance with the ability of the solid-state nanopore sensing to collect and analyze information on proteins, e.g., charge, size, shape, and complexation with other molecules, various properties of proteins have been studied in the nanopore field.

In 1987, Singer et al. reported the first idea of the protein translocation through a biological nanopore.[163] The early sketch of the idea, translocation of a peptide molecule with a few subdomains through a translocator protein inserted in the lipid bilayer, conceptually indicated the feasibility of detecting protein translocation by means of the biological nanopore. Nevertheless, the translocation of a single protein molecule in a nanopore emerged in the 2000s, owing to the difficulties in protein translocation through α-hemolysin nanopore and the fabrication of the solid-state nanopore device. In 2006, Han et al. first reported protein translocation through the solid-state nanopore.[160] Translocation of a single bovine serum albumin (BSA) protein molecule across a 20 nm thick SiN membrane with a 50 nm diameter pore was detected. The nanopore structure with relatively large pore sizes (in comparison with the devices used for DNA experiments) or with the dimensions comparable to those of the analyte proteins was widely accepted and similarly adopted in other studies on the nanopore protein detection.

Figure 13 depicts selected works on protein translocation in the solid-state nanopore. A property of a protein that determines its translocation through the nanopore is the net charge; protein molecules generally have relatively low charge density in total as compared to DNA. Therefore, the net charge of proteins can be easily modified or even the sign of the charge can be switched by a slight change in the electrolyte pH. On the basis of this phenomenon, Firnkes et al. investigated the changes in the translocation mode according to the net charge conversion of avidin and the SiN pore wall at different solution pH levels (Figure 13a).[158] The effect of the pH on the event frequency of avidin translocation through a nanopore was experimentally determined; the change in the event frequency was due to the balance between the electroosmotic flow velocity generated by the electric double layer near SiN and the electrophoretic velocity of avidin. Likewise, Steinbock et al. and Fologea et al. demonstrated conversion of the net charge of BSA and its effect on nanopore translocation events, by shifting pH of the electrolyte above or below the isoelectric point (pI) of BSA (pI = 4.7).[7,159] These results suggest that a change in the zeta potential of a protein and the pore wall under the influence of pH is useful for controlling the mode of translocation and the translocation rate.

Another important feature of a protein that is resolvable by the solid-state nanopore is the conformation or the size of the protein. Several studies in the field of solid-state nanopore have distinguished protein conformation change before and after its full denaturation.[69,140,164] Without degrading the protein functionality, Yusko et al. identified differently sized Aβ aggregates as spherical oligomers, protofibrils, or mature fibers according to their translocation signals in the lipid-coated solid-state nanopore (Figure 13b).[140] They proved the feasibility of size discrimination among heterogeneous Aβ aggregates in solution using the solid-state nanopore. Moreover, the particle size characterization principle enabled profiling of the kinetic process of Aβ fibrilization by monitoring the event frequency of each Aβ aggregates. Consumption of small oligomers in the fibrilization process was reflected in a decrease in its event frequency over time, while the frequency of the translocation events for the mature fibril increased from day 0 to day 3. The trend of the protein conformation change observed using the solid-state nanopore was in agreement with the electron microscopy images of Aβ taken in the same time periods.

Li et al. attempted discrimination of several proteins of different sizes, with their molecular weights ranging from 14 to 465 kDa, by means of the glass nanocapillaries.[72] The protein detection using the low-noise glass-based nanopore was successful in this work. Nonetheless, the protein size could not be clearly discriminated because of too fast translocation of proteins accompanied by signal distortion by the lowpass filter. Similarly, Steinbock et al. also succeeded in distinguishing proteins of 12–480 kDa by means of glass nanocapillaries (Figure 13c).[7] Although they applied a 10 kHz Bessel filter to process the ionic current signals, differentiating the scatter plots of conductance drop versus dwell time for each protein was possible because they fabricated a glass nanopore with a diameter as small as the target proteins to enhance the SNR.

Although numerous studies on single-protein characterization using the solid-state nanopore revealed biophysical properties of proteins, detecting the fast translocation of a protein is still limited by the insufficient temporal resolution of the measurement system. Plesa et al. explored the nanopore detection limit for each protein with molecular weights ranging from 6 to 660 kDa.[162] Using a 1D first-passage time-distribution model,[37,69,165] they calculated the event loss ratio as a function of the drift velocity of the proteins and the diffusion coefficient (Figure 13d).[162] They revealed that application of the 10 kHz lowpass Bessel filter caused a severe loss of the translocation signals because of the temporal resolution limit, suggesting that an amplifier with a higher data acquisition frequency is required for protein detection. Subsequently, Larkin et al. employed a high bandwidth amplifier sampling the ionic current signals at a 4 MHz frequency and filtering the high-frequency signals at 250 kHz (Figure 13e).[68] They concluded that with the signal amplifier having the MHz bandwidth, 30–80% of the events were detected among RNase translocation events, and 70–90% of the events were detected among proteinase K (ProtK) translocations. These studies qualitatively and quantitatively indicate that proteins with molecular weight <50 kDa cross the nanopore at undetectably fast velocity and cause severe distortion in the translocation signals. Accordingly, to improve the resolution of protein translocation events in the solid-state nanopore, it is necessary to use a high-frequency amplifier and a nanopore device with low electrical noise even at high-frequency range.

As an effort to physically understand the protein translocations, progresses in the protein analysis using nanopores have noticed the role of electroosmotic flow in the transport.[158,166]

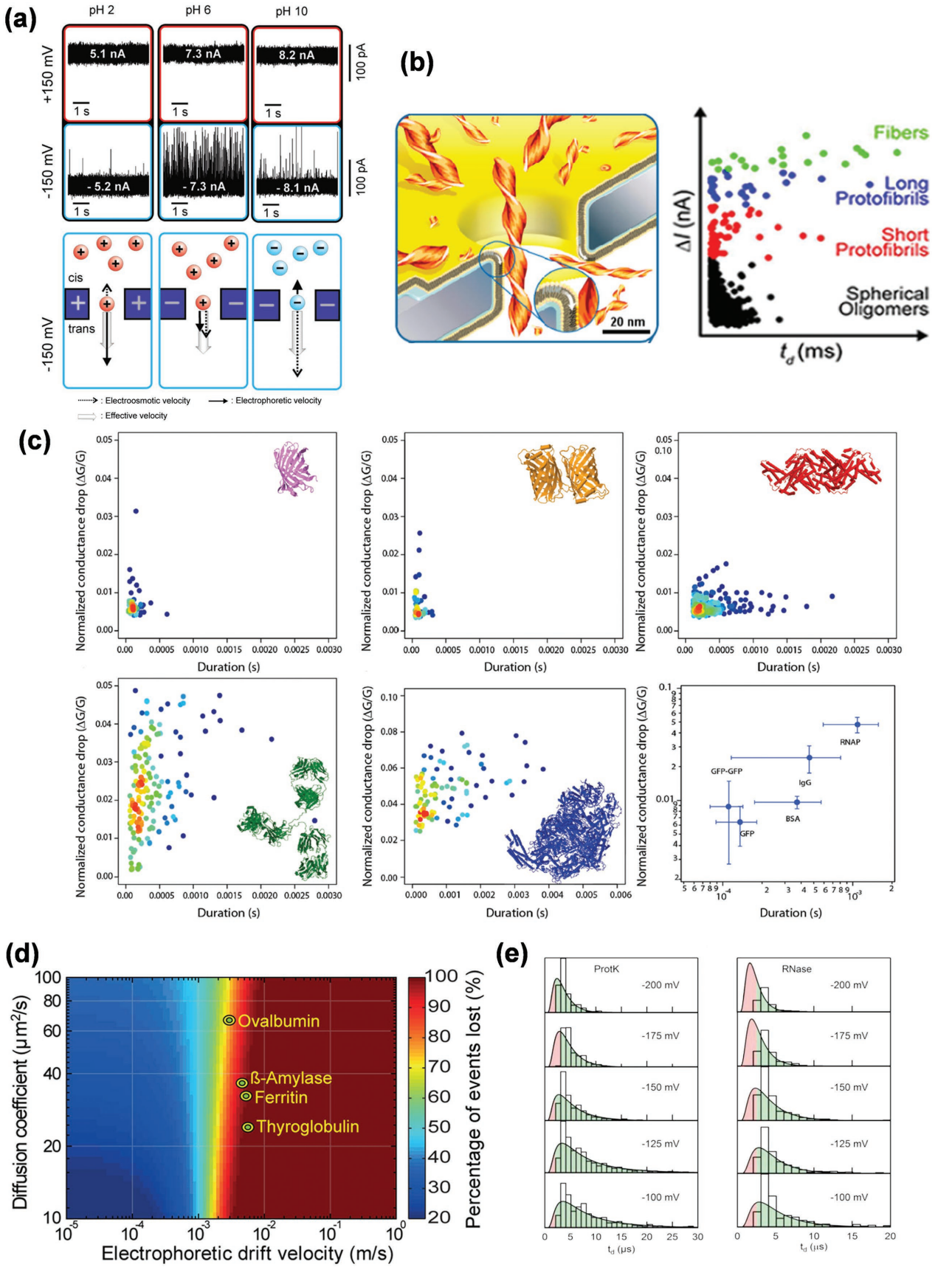

Waduge et al. claimed that the electroosmotic flow is as important as the electrophoretic force in the nanopore transport of proteins, and in their experiment, the former was even dominant.[167] Proteins have less electrical charge and lower electrophoretic mobility than DNA, and the influence of the electroosmotic flow becomes recognizable or even overtakes the effect of the electrophoretic force during the protein translocation. Therefore, understanding and controlling the electroosmotic factor is crucial in the analysis of protein translocation signals in the nanopore experiments.

Arising from the detection of single proteins and protein size discrimination, analysis of protein–protein interactions (PPIs) via detection of protein–protein complexes is another branch of the protein-based application of the solid-state nanopore.[65,70,123,138,168,169] The works on the detection of protein–protein complexes based on PPIs using the solid-state nanopore are graphically presented in **Figure 14**. PPIs originate from specific binding between different proteins, which is the most important and the most basic physiological function of proteins. On the basis of this feature, Uram et al. observed changes in the nanopore signals due to binding of an antibody and virus (Figure 14a).[168] They discriminated the signals generated by the virus (PBCV-1) and by the complex of antibodies (antiserum) with the virus; the increase of the volume of the particle after binding increased the peak amplitude. They also analyzed the binding kinetics of the antibodies and viruses quantitatively by examining the changes in the peak amplitude over time. Using the same principle, Freedman et al. detected the binding of HIV antigen gp120 and its antibody using the nanopore signals.[70] For more practical applications, they studied heterogeneous protein samples of the antibody+gp120 mixture, antibody+BSA mixture, antibody+gp120+BSA, and antibody+gp120+fetal bovine serum (FBS) (Figure 14b).[70] They confirmed that the additional distribution of the current drop from the translocation of the antibody–gp120 complex appeared at a larger ΔI, verifying the formation of the complex. In addition, they demonstrated that the interaction between BSA and the antibody was nonexistent by matching the current drop value observed during the biomolecule translocation for the antibody and for the antibody+BSA mixture. These studies have shown the possibility of nanopore sensors as a tool for future drug design, where complicated procedures such as molecular immobilization and labeling in the existing immunoassays are unnecessary.

A new approach was attempted by Kwak et al., who proposed a new drug screening strategy by examining a protein-small molecule interaction using the solid-state nanopore.[65] Although previously, the criterion for the detection of the PPI was a change in the current amplitude of the translocation signal, they detected the interaction between two proteins (globular glutathione-S-transferase (GST)-tagged p53TAD (GST-p53TAD) and mouse double minute 2 (MDM2) protein) by monitoring the event frequency change (Figure 14c).[65] MDM2 selectively binds to p53 and inhibits the functioning of this tumor suppressor protein, thus disabling the defense system of the body against cancerous cells.[170] The positively charged protein MDM2 relocated to the negatively biased chamber, but upon the complex formation, translocation of the MDM2–GST-p53TAD complex was inhibited by the net charge conversion of the complex from positive to negative. Here, the role of GST protein was to enhance the current blockade magnitude of the intrinsically disordered form of p53. Moreover, they demonstrated restoration of the MDM2 signal by addition of nutlin-3 (a drug candidate for repairing p53 activity), thus freeing the proteins from binding.[65]

Therefore, this ultrasensitive nanopore-based drug screening strategy showed its superiority to the current technology with limitations such as insufficient specificity of the enzyme-targeted method, fluorophore labeling for fluorescence polarization, and a large amount of protein required for NMR. Nanopore detection of single protein molecules and protein–protein complexes is the consequence of the improvement in the nanopore device and the electrical amplifier, namely reduced electrical noise and enhanced temporal resolution. Nevertheless, a similar goal still remains as in the detection of DNA–protein complexes and modified DNA structures: for even more sensitive and accurate detection of proteins, the spatial and temporal resolution should be further enhanced by improving the digital setup of nanopore experiments and by slowing the translocation speed of proteins.

4. Conclusion and Future Prospects

Herein, the fundamental principles, developments, and applications of the solid-state nanopore are summarized, with the emphasis on the device and its performance characteristics including the electrical noise properties and the spatial and temporal resolution. The solid-state nanopore has emerged as a fabricated version of the biological nanopore with its manufacturability, mechanical and chemical stability, and flexibility in the nanopore dimensions. The improvements in the resolution of the solid-state nanopore devices have been achieved by applying dielectric materials, by increasing the bandwidth of the ionic current measurement, and by means of 2D materials as the nanopore membrane. Furthermore, via organic coating or hybridization with the biological nanopore, chemical functionalities related to the biomolecule transport could be integrated into the solid-state nanopore. Finally, the recently reported applications of the solid-state nanopore were categorized and

Figure 13. Single-molecule protein characterization using the solid-state nanopore. a) Avidin translocation through a SiN nanopore at different pH levels in solution and corresponding charge states of avidin and SiN wall. b) Aβ conformation analysis using a lipid bilayer-coated nanopore based on ΔI of translocation signals. c) Scatter plots of translocation duration versus normalized conductance drop for proteins studied using the glass capillary nanopores. Each scatter plot represents translocation events of green fluorescent protein (GFP, pink), GFP–GFP dimer (FP, orange), BSA (red), IgG (green), and RNA polymerase (RNAp, navy). All the results are summarized in the rightmost graph in the second row. d) The nanopore detection limit on the mapping of a protein expressed as the interplay of the in-pore molecular diffusivity and the electrophoretic drift velocity. e) Nanopore translocation time histogram of proteinase K (left) and RNase (right) at 100–200 mV, with red-shadowed regions indicating the signal loss caused by limited temporal resolution of a nanopore. The y-axis shows arbitrary units. a) Reproduced with permission.[158] Copyright 2010, American Chemical Society; b) Reproduced with permission.[140] Copyright 2012, American Chemical Society; c) Reproduced with permission.[7] Copyright 2014, Royal Society of Chemistry; d) Reproduced with permission.[162] Copyright 2013, American Chemical Society; e) Reproduced with permission.[68] Copyright 2014, Elsevier.

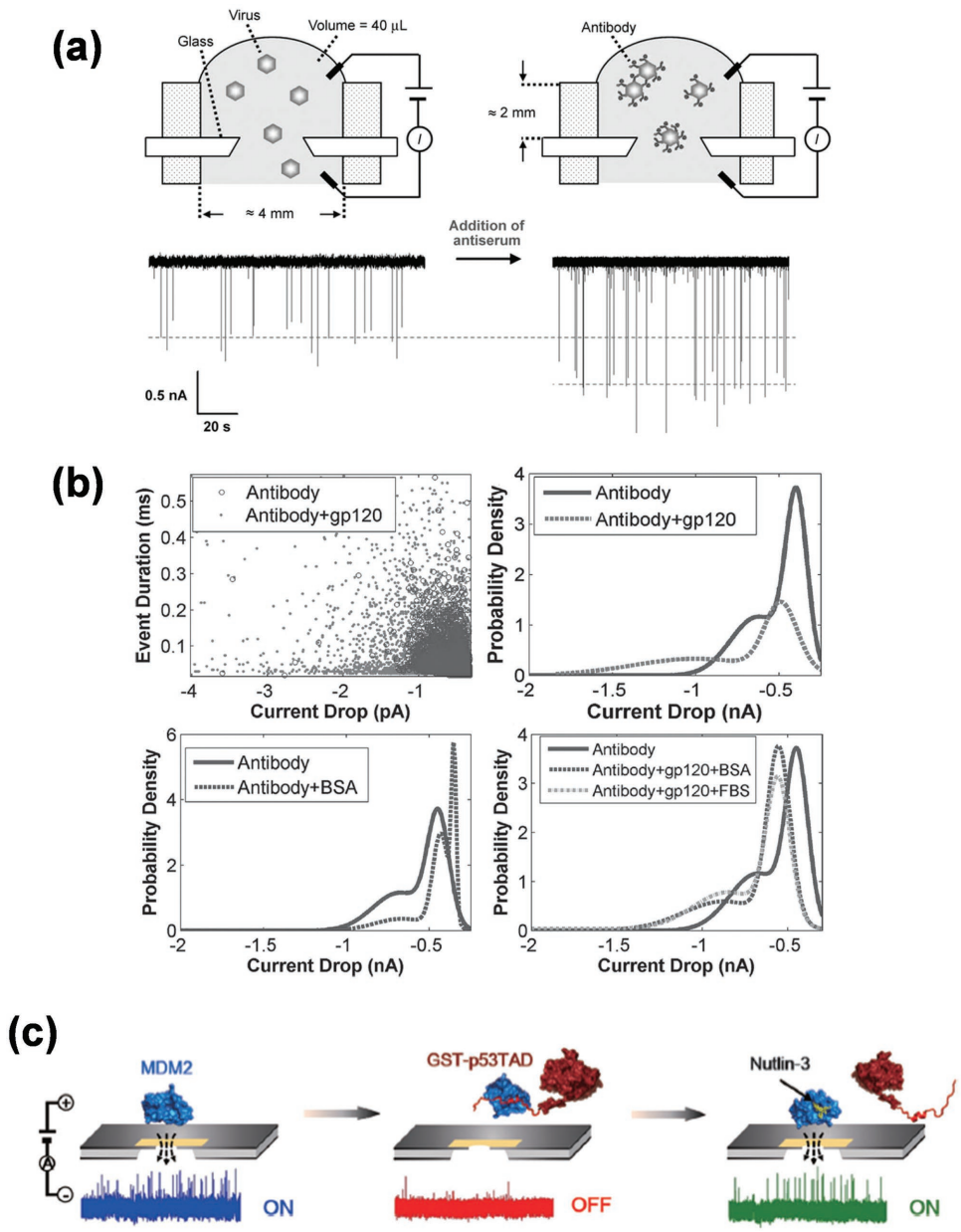

Figure 14. Protein–protein interaction analysis. a) Analysis of the antibody–PBCV-1 virus interaction using the glass nanopore and resulting translocation signals. b) Analysis of the HIV antigen gp120, an antibody, and a protein (BSA and FBS) using the nanopore according to the current drop magnitude. c) Nanopore-based analysis of inhibition of the p53–MDM2 interaction by a drug (nutlin-3). The cartoons on the interactions between molecules and resulting translocation signals are presented. a) Reproduced with permission.[168] Copyright 2006, Wiley-VCH; b) Reproduced with permission.[70] Copyright 2013, Wiley-VCH; c) Adapted with permission.[65] Copyright 2016, Wiley-VCH.

described here by target molecules: DNA-bound proteins, modified DNA structures, proteins, and protein–protein complexes.

Among the limitations discussed in Section 1.4, the resolution of the solid-state nanopore has been dealt with extensively from the standpoint of devices and materials as presented in Section 2. The reliability of the device, however, resistance to nanopore clogging by nonspecifically adsorbed molecules on the nanopore surface in particular, has some room for improvement. This issue is directly related to the efficiency of a solid-state nanopore device because the expected lifetime of the device and the number of the translocation events detected by the nanopore may be strongly limited by the adsorption of unwanted DNA or proteins. In Section 2.2.2, we introduced the early-stage reports on the PEG self-assembly coating of the nanopore surface to prevent adsorption to the pore and to maximize the expected lifetime of the device.[103,104] This approach, or any other novel ideas about the enhancement of the device reliability, can be further improved and optimized for stable, robust, and long-lasting use of the solid-state nanopore.

With further improvements in the device resolution and reliability, the solid-state nanopore may approach the challenges in this field. The challenging topics include DNA base

discrimination, protein sequencing by detecting the sequence-specifically bound proteins, and drug screening. In these applications, the nanopores are required to detect and resolve small features, even small as a couple of nanometers or less in size. In addition, ssDNA and proteins cause severe pore clogging compared to dsDNA, so the importance of fabricating antiadsorptive devices would be emphasized.

In addition to the reliability, there are a few issues to be resolved regarding the optimization, productization, and commercialization of the solid-state nanopore. The solid-state nanopores should be mass produced with uniform device properties and performances and may be multiplexed for higher throughput detection or DNA sequencing. Actually, these directions for improvement of the solid-state nanopore are influenced by the commercialized biological nanopore sequencing platforms, which are now well established in the global market for next-generation DNA sequencing. Representatively, Oxford Nanopore Technologies solutions include thousands separate nanopore channels, where the biological nanopores and the membrane have the uniform dimensions and structures across the platform. Therefore, the future solid-state nanopore can mimic the design of the biological nanopore sequencers. For instance, among the techniques discussed in this review, the CDB method and e-beam lithography are more suitable than the TEM-based method for mass production and multiplexing of nanopores. Likewise, other breakthroughs and developments in the solid-state nanopores may be introduced into the field in the near future, and contribute to the commercial use of the platform as an accurate, fast, and reliable biomolecule sensor.

Acknowledgements

This work was supported by the Pioneer Research Center Program through the National Research Foundation of Korea funded by the Ministry of Science and ICT (MSIT) of Korea (2012-0009563), and by the BioNano Health-Guard Research Center funded by the Ministry of Science and ICT (MSIT) of Korea as Global Frontier Project (H-GUARD _2014M3A6B2060301).

Conflict of Interest

The authors declare no conflict of interest.

Keywords

DNA sequencing, nanopore devices, nanopore fabrication, solid-state nanopores

Received: August 17, 2017
Revised: June 8, 2018
Published online:

[1] J. J. Kasianowicz, E. Brandin, D. Branton, D. W. Deamer, *Proc. Natl. Acad. Sci. USA* **1996**, *93*, 13770.
[2] C. Dekker, *Nat. Nanotechnol.* **2007**, *2*, 209.
[3] M. Wanunu, *Phys. Life Rev.* **2012**, *9*, 125.
[4] A. Meller, L. Nivon, E. Brandin, J. Golovchenko, D. Branton, *Proc. Natl. Acad. Sci. USA* **2000**, *97*, 1079.
[5] M. Wanunu, T. Dadosh, V. Ray, J. Jin, L. McReynolds, M. Drndic, *Nat. Nanotechnol.* **2010**, *5*, 807.
[6] M. Akeson, D. Branton, J. J. Kasianowicz, E. Brandin, D. W. Deamer, *Biophys. J.* **1999**, *77*, 3227.
[7] L. J. Steinbock, S. Krishnan, R. D. Bulushev, S. Borgeaud, M. Blokesch, L. Feletti, A. Radenovic, *Nanoscale* **2014**, *6*, 14380.
[8] M. H. Lee, A. Kumar, K. B. Park, S. Y. Cho, H. M. Kim, M. C. Lim, Y. R. Kim, K. B. Kim, *Sci. Rep.* **2014**, *4*, 7448.
[9] M. Wanunu, W. Morrison, Y. Rabin, A. Y. Grosberg, A. Meller, *Nat. Nanotechnol.* **2010**, *5*, 160.
[10] A. Darvish, G. Goyal, R. Aneja, R. V. Sundaram, K. Lee, C. W. Ahn, K. B. Kim, P. M. Vlahovska, M. J. Kim, *Nanoscale* **2016**, *8*, 14420.
[11] D. W. Deamer, M. Akeson, *Trends Biotechnol.* **2000**, *18*, 147.
[12] B. M. Venkatesan, R. Bashir, *Nat. Nanotechnol.* **2011**, *6*, 615.
[13] a) M. Tsutsui, M. Taniguchi, K. Yokota, T. Kawai, *Nat. Nanotechnol.* **2010**, *5*, 286; b) A. P. Ivanov, E. Instuli, C. M. McGilvery, G. Baldwin, D. W. McComb, T. Albrecht, J. B. Edel, *Nano Lett.* **2011**, *11*, 279.
[14] a) G. A. Chansin, R. Mulero, J. Hong, M. J. Kim, A. J. DeMello, J. B. Edel, *Nano Lett.* **2007**, *7*, 2901; b) G. Ando, C. Hyun, J. Li, T. Mitsui, *ACS Nano* **2012**, *6*, 10090.
[15] W. H. Pitchford, H. J. Kim, A. P. Ivanov, H. M. Kim, J. S. Yu, R. J. Leatherbarrow, T. Albrecht, K. B. Kim, J. B. Edel, *ACS Nano* **2015**, *9*, 1740.
[16] J. Li, D. Stein, C. McMullan, D. Branton, M. J. Aziz, J. A. Golovchenko, *Nature* **2001**, *412*, 166.
[17] A. J. Storm, J. H. Chen, X. S. Ling, H. W. Zandbergen, C. Dekker, *Nat. Mater.* **2003**, *2*, 537.
[18] D. Branton, D. W. Deamer, A. Marziali, H. Bayley, S. A. Benner, T. Butler, M. Di Ventra, S. Garaj, A. Hibbs, X. Huang, S. B. Jovanovich, P. S. Krstic, S. Lindsay, X. S. Ling, C. H. Mastrangelo, A. Meller, J. S. Oliver, Y. V. Pershin, J. M. Ramsey, R. Riehn, G. V. Soni, V. Tabard-Cossa, M. Wanunu, M. Wiggin, J. A. Schloss, *Nat. Biotechnol.* **2008**, *26*, 1146.
[19] D. H. Stoloff, M. Wanunu, *Curr. Opin. Biotechnol.* **2013**, *24*, 699.
[20] A. H. Squires, T. Gilboa, C. Torfstein, N. Varongchayakul, A. Meller, in *Methods in Enzymology*, Vol. *582* (Ed: C. Ziegler), Academic Press, Cambridge, MA, USA **2017**, p. 353.
[21] J. Li, D. P. Yu, Q. Zhao, *Microchim. Acta* **2016**, *183*, 941.
[22] D. Deamer, M. Akeson, D. Branton, *Nat. Biotechnol.* **2016**, *34*, 518.
[23] G. Church, D. W. Deamer, D. Branton, R. Baldarelli, J. Kasianowicz, *US5795782 A*, **1998**.
[24] a) D. W. Deamer, D. Branton, *Acc. Chem. Res.* **2002**, *35*, 817; b) T. Z. Butler, J. H. Gundlach, M. Troll, *Biophys. J.* **2007**, *93*, 3229.
[25] M. Rhee, M. A. Burns, *Trends Biotechnol.* **2007**, *25*, 174.
[26] a) S. Howorka, S. Cheley, H. Bayley, *Nat. Biotechnol.* **2001**, *19*, 636; b) W. Vercoutere, S. Winters-Hilt, H. Olsen, D. Deamer, D. Haussler, M. Akeson, *Nat. Biotechnol.* **2001**, *19*, 248.
[27] I. M. Derrington, T. Z. Butler, M. D. Collins, E. Manrao, M. Pavlenok, M. Niederweis, J. H. Gundlach, *Proc. Natl. Acad. Sci USA* **2010**, *107*, 16060.
[28] G. M. Cherf, K. R. Lieberman, H. Rashid, C. E. Lam, K. Karplus, M. Akeson, *Nat. Biotechnol.* **2012**, *30*, 344.
[29] E. A. Manrao, I. M. Derrington, A. H. Laszlo, K. W. Langford, M. K. Hopper, N. Gillgren, M. Pavlenok, M. Niederweis, J. H. Gundlach, *Nat. Biotechnol.* **2012**, *30*, 349.
[30] G. F. Schneider, C. Dekker, *Nat. Biotechnol.* **2012**, *30*, 326.
[31] T. Z. Butler, M. Pavlenok, I. M. Derrington, M. Niederweis, J. H. Gundlach, *Proc. Natl. Acad. Sci. USA* **2008**, *105*, 20647.
[32] a) M. Soskine, A. Biesemans, B. Moeyaert, S. Cheley, H. Bayley, G. Maglia, *Nano Lett.* **2012**, *12*, 4895; b) M. Soskine, A. Biesemans, M. De Maeyer, G. Maglia, *J. Am. Chem. Soc.* **2013**, *135*, 13456; c) M. Soskine, A. Biesemans, G. Maglia, *J. Am. Chem. Soc.* **2015**, *137*, 5793.

[33] a) D. Wendell, P. Jing, J. Geng, V. Subramaniam, T. J. Lee, C. Montemagno, P. Guo, *Nat. Nanotechnol.* **2009**, *4*, 765; b) F. Haque, J. Lunn, H. Fang, D. Smithrud, P. Guo, *ACS Nano* **2012**, *6*, 3251; c) F. Haque, J. Li, H.-C. Wu, X.-J. Liang, P. Guo, *Nano Today* **2013**, *8*, 56; d) Z. Ji, S. Wang, Z. Zhao, Z. Zhou, F. Haque, P. Guo, *Small* **2016**, *12*, 4572.
[34] a) Z. Zhou, Z. Ji, S. Wang, F. Haque, P. Guo, *Biomaterials* **2016**, *105*, 222; b) S. Wang, Z. Zhou, Z. Zhao, H. Zhang, F. Haque, P. Guo, *Biomaterials* **2017**, *126*, 10.
[35] a) R. Stefureac, Y.-t. Long, H.-B. Kraatz, P. Howard, J. S. Lee, *Biochemistry* **2006**, *45*, 9172; b) C. Cao, J. Yu, Y.-Q. Wang, Y.-L. Ying, Y.-T. Long, *Anal. Chem.* **2016**, *88*, 5046.
[36] D. Fologea, J. Uplinger, B. Thomas, D. S. McNabb, J. Li, *Nano Lett.* **2005**, *5*, 1734.
[37] J. Li, D. S. Talaga, *J. Phys.: Condens. Matter* **2010**, *22*, 454129.
[38] S. W. Kowalczyk, D. B. Wells, A. Aksimentiev, C. Dekker, *Nano Lett.* **2012**, *12*, 1038.
[39] a) U. F. Keyser, J. van der Does, C. Dekker, N. H. Dekker, *Rev. Sci. Instrum.* **2006**, *77*, 105105; b) C. Hyun, H. Kaur, R. Rollings, M. Xiao, J. Li, *ACS Nano* **2013**, *7*, 5892.
[40] U. F. Keyser, B. N. Koeleman, S. Van Dorp, D. Krapf, R. M. M. Smeets, S. G. Lemay, N. H. Dekker, C. Dekker, *Nat. Phys.* **2006**, *2*, 473.
[41] a) Y. He, M. Tsutsui, C. Fan, M. Taniguchi, T. Kawai, *ACS Nano* **2011**, *5*, 5509; b) Y. He, M. Tsutsui, C. Fan, M. Taniguchi, T. Kawai, *ACS Nano* **2011**, *5*, 8391.
[42] S. Banerjee, J. Wilson, J. Shim, M. Shankla, E. A. Corbin, A. Aksimentiev, R. Bashir, *Adv. Funct. Mater.* **2015**, *25*, 936.
[43] J. Larkin, R. Henley, D. C. Bell, T. Cohen-Karni, J. K. Rosenstein, M. Wanunu, *ACS Nano* **2013**, *7*, 10121.
[44] P. Krishnakumar, B. Gyarfas, W. Song, S. Sen, P. Zhang, P. Krstic, S. Lindsay, *ACS Nano* **2013**, *7*, 10319.
[45] A. H. Squires, J. S. Hersey, M. W. Grinstaff, A. Meller, *J. Am. Chem. Soc.* **2013**, *135*, 16304.
[46] K.-B. Park, H.-J. Kim, Y.-H. Kang, J.-S. Yu, H. Chae, K. Lee, H.-M. Kim, K.-B. Kim, *Nanoscale* **2017**, *9*, 18772.
[47] S. Garaj, W. Hubbard, A. Reina, J. Kong, D. Branton, J. A. Golovchenko, *Nature* **2010**, *467*, 190.
[48] C. A. Merchant, K. Healy, M. Wanunu, V. Ray, N. Peterman, J. Bartel, M. D. Fischbein, K. Venta, Z. Luo, A. T. Johnson, M. Drndic, *Nano Lett.* **2010**, *10*, 2915.
[49] G. F. Schneider, S. W. Kowalczyk, V. E. Calado, G. Pandraud, H. W. Zandbergen, L. M. Vandersypen, C. Dekker, *Nano Lett.* **2010**, *10*, 3163.
[50] S. Liu, B. Lu, Q. Zhao, J. Li, T. Gao, Y. Chen, Y. Zhang, Z. Liu, Z. Fan, F. Yang, L. You, D. Yu, *Adv. Mater.* **2013**, *25*, 4549.
[51] Z. Zhou, Y. Hu, H. Wang, Z. Xu, W. L. Wang, X. D. Bai, X. Y. Shan, X. H. Lu, *Sci. Rep.* **2013**, *3*, 3287.
[52] K. B. Park, H. J. Kim, H. M. Kim, S. A. Han, K. H. Lee, S. W. Kim, K. B. Kim, *Nanoscale* **2016**, *8*, 5755.
[53] J. Feng, K. Liu, R. D. Bulushev, S. Khlybov, D. Dumcenco, A. Kis, A. Radenovic, *Nat. Nanotechnol.* **2015**, *10*, 1070.
[54] J. Feng, K. Liu, M. Graf, M. Lihter, R. D. Bulushev, D. Dumcenco, D. T. Alexander, D. Krasnozhon, T. Vuletic, A. Kis, A. Radenovic, *Nano Lett.* **2015**, *15*, 3431.
[55] P. Waduge, I. Bilgin, J. Larkin, R. Y. Henley, K. Goodfellow, A. C. Graham, D. C. Bell, N. Vamivakas, S. Kar, M. Wanunu, *ACS Nano* **2015**, *9*, 7352.
[56] K. Venta, G. Shemer, M. Puster, J. A. Rodriguez-Manzo, A. Balan, J. K. Rosenstein, K. Shepard, M. Drndic, *ACS Nano* **2013**, *7*, 4629.
[57] V. Tabard-Cossa, D. Trivedi, M. Wiggin, N. N. Jetha, A. Marziali, *Nanotechnology* **2007**, *18*, 305505.
[58] T. Jain, R. J. Guerrero, C. A. Aguilar, R. Karnik, *Anal. Chem.* **2013**, *85*, 3871.
[59] J. K. Rosenstein, M. Wanunu, C. A. Merchant, M. Drndic, K. L. Shepard, *Nat. Methods* **2012**, *9*, 487.
[60] A. Balan, B. Machielse, D. Niedzwiecki, J. Lin, P. Ong, R. Engelke, K. L. Shepard, M. Drndic, *Nano Lett.* **2014**, *14*, 7215.
[61] S. Shekar, D. J. Niedzwiecki, C. C. Chien, P. Ong, D. A. Fleischer, J. Lin, J. K. Rosenstein, M. Drndic, K. L. Shepard, *Nano Lett.* **2016**, *16*, 4483.
[62] J. S. Yu, M. C. Lim, D. T. Huynh, H. J. Kim, H. M. Kim, Y. R. Kim, K. B. Kim, *ACS Nano* **2015**, *9*, 5289.
[63] A. Squires, E. Atas, A. Meller, *Sci. Rep.* **2015**, *5*, 11643.
[64] J. Shim, G. I. Humphreys, B. M. Venkatesan, J. M. Munz, X. Zou, C. Sathe, K. Schulten, F. Kosari, A. M. Nardulli, G. Vasmatzis, R. Bashir, *Sci. Rep.* **2013**, *3*, 1389.
[65] D. K. Kwak, H. Chae, M. K. Lee, J. H. Ha, G. Goyal, M. J. Kim, K. B. Kim, S. W. Chi, *Angew. Chem., Int. Ed. Engl.* **2016**, *55*, 5713.
[66] A. J. Storm, J. H. Chen, H. W. Zandbergen, C. Dekker, *Phys. Rev. E: Stat., Nonlinear, Soft Matter Phys.* **2005**, *71*, 051903.
[67] J. Li, M. Gershow, D. Stein, E. Brandin, J. A. Golovchenko, *Nat. Mater.* **2003**, *2*, 611.
[68] J. Larkin, R. Y. Henley, M. Muthukumar, J. K. Rosenstein, M. Wanunu, *Biophys. J.* **2014**, *106*, 696.
[69] D. S. Talaga, J. Li, *J. Am. Chem. Soc.* **2009**, *131*, 9287.
[70] K. J. Freedman, A. R. Bastian, I. Chaiken, M. J. Kim, *Small* **2013**, *9*, 750.
[71] L. J. Steinbock, R. D. Bulushev, S. Krishnan, C. Raillon, A. Radenovic, *ACS Nano* **2013**, *7*, 11255.
[72] W. Li, N. A. Bell, S. Hernandez-Ainsa, V. V. Thacker, A. M. Thackray, R. Bujdoso, U. F. Keyser, *ACS Nano* **2013**, *7*, 4129.
[73] a) R. L. Fraccari, P. Ciccarella, A. Bahrami, M. Carminati, G. Ferrari, T. Albrecht, *Nanoscale* **2016**, *8*, 7604; b) P. Cadinu, B. Paulose Nadappuram, D. J. Lee, J. Y. Y. Sze, G. Campolo, Y. Zhang, A. Shevchuk, S. Ladame, T. Albrecht, Y. Korchev, A. P. Ivanov, J. B. Edel, *Nano Lett.* **2017**, *17*, 6376.
[74] R. L. Fraccari, M. Carminati, G. Piantanida, T. Leontidou, G. Ferrari, T. Albrecht, *Faraday Discuss.* **2016**, *193*, 459.
[75] N. A. Bell, U. F. Keyser, *J. Am. Chem. Soc.* **2015**, *137*, 2035.
[76] N. A. Bell, U. F. Keyser, *Nat. Nanotechnol.* **2016**, *11*, 645.
[77] J. Kong, N. A. Bell, U. F. Keyser, *Nano Lett.* **2016**, *16*, 3557.
[78] C. R. Crick, P. Albella, H.-J. Kim, A. P. Ivanov, K.-B. Kim, S. A. Maier, J. B. Edel, *ACS Photonics* **2017**, *4*, 2835.
[79] J. Larkin, R. Y. Henley, V. Jadhav, J. Korlach, M. Wanunu, *Nat. Nanotechnol.* **2017**, *12*, 1169.
[80] a) M. Jain, H. E. Olsen, B. Paten, M. Akeson, *Genome Biol.* **2016**, *17*, 239; b) E. C. Hayden, *Nature News*, https://doi.org/10.1038/nature.2014.14724 (accessed: December 2017).
[81] J. Wang, N. E. Moore, Y. M. Deng, D. A. Eccles, R. J. Hall, *Front. Microbiol.* **2015**, *6*, 766.
[82] J. Quick, N. J. Loman, S. Duraffour, J. T. Simpson, E. Severi, L. Cowley, J. A. Bore, R. Koundouno, G. Dudas, A. Mikhail, N. Ouedraogo, B. Afrough, A. Bah, J. H. Baum, B. Becker-Ziaja, J. P. Boettcher, M. Cabeza-Cabrerizo, A. Camino-Sanchez, L. L. Carter, J. Doerrbecker, T. Enkirch, I. G. G. Dorival, N. Hetzelt, J. Hinzmann, T. Holm, L. E. Kafetzopoulou, M. Koropogui, A. Kosgey, E. Kuisma, C. H. Logue, A. Mazzarelli, S. Meisel, M. Mertens, J. Michel, D. Ngabo, K. Nitzsche, E. Pallash, L. V. Patrono, J. Portmann, J. G. Repits, N. Y. Rickett, A. Sachse, K. Singethan, I. Vitoriano, R. L. Yemanaberhan, E. G. Zekeng, R. Trina, A. Bello, A. A. Sall, O. Faye, O. Faye, N. Magassouba, C. V. Williams, V. Amburgey, L. Winona, E. Davis, J. Gerlach, F. Washington, V. Monteil, M. Jourdain, M. Bererd, A. Camara, H. Somlare, A. Camara, M. Gerard, G. Bado, B. Baillet, D. Delaune, K. Y. Nebie, A. Diarra, Y. Savane, R. B. Pallawo, G. J. Gutierrez, N. Milhano, I. Roger, C. J. Williams, F. Yattara, K. Lewandowski, J. Taylor, P. Rachwal, D. Turner, G. Pollakis, J. A. Hiscox, D. A. Matthews, M. K. O'Shea, A. M. Johnston, D. Wilson, E. Hutley, E. Smit, A. Di Caro, R. Woelfel, K. Stoecker,

E. Fleischmann, M. Gabriel, S. A. Weller, L. Koivogui, B. Diallo, S. Keita, A. Rambaut, P. Formenty, S. Gunther, M. W. Carroll, *Nature* **2016**, *530*, 228.

[83] N. R. Faria, J. Quick, I. M. Claro, J. Theze, J. G. de Jesus, M. Giovanetti, M. U. G. Kraemer, S. C. Hill, A. Black, A. C. da Costa, L. C. Franco, S. P. Silva, C. H. Wu, J. Raghwani, S. Cauchemez, L. du Plessis, M. P. Verotti, W. K. de Oliveira, E. H. Carmo, G. E. Coelho, A. Santelli, L. C. Vinhal, C. M. Henriques, J. T. Simpson, M. Loose, K. G. Andersen, N. D. Grubaugh, S. Somasekar, C. Y. Chiu, J. E. Munoz-Medina, C. R. Gonzalez-Bonilla, C. F. Arias, L. L. Lewis-Ximenez, S. A. Baylis, A. O. Chieppe, S. F. Aguiar, C. A. Fernandes, P. S. Lemos, B. L. S. Nascimento, H. A. O. Monteiro, I. C. Siqueira, M. G. de Queiroz, T. R. de Souza, J. F. Bezerra, M. R. Lemos, G. F. Pereira, D. Loudal, L. C. Moura, R. Dhalia, R. F. Franca, T. Magalhaes, E. T. Marques Jr., T. Jaenisch, G. L. Wallau, M. C. de Lima, V. Nascimento, E. M. de Cerqueira, M. M. de Lima, D. L. Mascarenhas, J. P. M. Neto, A. S. Levin, T. R. Tozetto-Mendoza, S. N. Fonseca, M. C. Mendes-Correa, F. P. Milagres, A. Segurado, E. C. Holmes, A. Rambaut, T. Bedford, M. R. T. Nunes, E. C. Sabino, L. C. J. Alcantara, N. J. Loman, O. G. Pybus, *Nature* **2017**, *546*, 406.

[84] J. B. Heng, C. Ho, T. Kim, R. Timp, A. Aksimentiev, Y. V. Grinkova, S. Sligar, K. Schulten, G. Timp, *Biophys. J.* **2004**, *87*, 2905.

[85] S. W. Kowalczyk, A. Y. Grosberg, Y. Rabin, C. Dekker, *Nanotechnology* **2011**, *22*, 315101.

[86] M. Wanunu, J. Sutin, B. McNally, A. Chow, A. Meller, *Biophys. J.* **2008**, *95*, 4716.

[87] H. Kwok, K. Briggs, V. Tabard-Cossa, *PLoS One* **2014**, *9*, e92880.

[88] A. Balan, C. C. Chien, R. Engelke, M. Drndic, *Sci. Rep.* **2015**, *5*, 17775.

[89] J. A. Bafna, G. V. Soni, *PLoS One* **2016**, *11*, e0157399.

[90] P. Chen, T. Mitsui, D. B. Farmer, J. Golovchenko, R. G. Gordon, D. Branton, *Nano Lett.* **2004**, *4*, 1333.

[91] A. Kumar, K. B. Park, H. M. Kim, K. B. Kim, *Nanotechnology* **2013**, *24*, 495503.

[92] K. Liu, J. Feng, A. Kis, A. Radenovic, *ACS Nano* **2014**, *8*, 2504.

[93] H. Kwok, M. Waugh, J. Bustamante, K. Briggs, V. Tabard-Cossa, *Adv. Funct. Mater.* **2014**, *24*, 7745.

[94] S. W. Nam, M. J. Rooks, K. B. Kim, S. M. Rossnagel, *Nano Lett.* **2009**, *9*, 2044.

[95] H. M. Kim, M. H. Lee, K. B. Kim, *Nanotechnology* **2011**, *22*, 275303.

[96] I. Yanagi, K. Fujisaki, H. Hamamura, K. Takeda, *J. Appl. Phys.* **2017**, *121*, 045301.

[97] K. Matsui, I. Yanagi, Y. Goto, K.-i. Takeda, *Sci. Rep.* **2015**, *5*, 17819.

[98] M. J. Kim, M. Wanunu, D. C. Bell, A. Meller, *Adv. Mater.* **2006**, *18*, 3149.

[99] M. J. Kim, B. McNally, K. Murata, A. Meller, *Nanotechnology* **2007**, *18*, 205302.

[100] N. A. W. Bell, K. Chen, S. Ghosal, M. Ricci, U. F. Keyser, *Nat. Commun.* **2017**, *8*, 380.

[101] S. Carson, J. Wilson, A. Aksimentiev, M. Wanunu, *Biophys. J.* **2014**, *107*, 2381.

[102] S. Lindsay, *Nat. Nanotechnol.* **2016**, *11*, 109.

[103] G. F. Schneider, Q. Xu, S. Hage, S. Luik, J. N. Spoor, S. Malladi, H. Zandbergen, C. Dekker, *Nat. Commun.* **2013**, *4*, 2619.

[104] Z. Tang, B. Lu, Q. Zhao, J. Wang, K. Luo, D. Yu, *Small* **2014**, *10*, 4332.

[105] Z. Liang, Z. Tang, J. Li, R. Hu, D. Yu, Q. Zhao, *Nanoscale* **2015**, *7*, 10752.

[106] D. J. Niedzwiecki, J. Grazul, L. Movileanu, *J. Am. Chem. Soc.* **2010**, *132*, 10816.

[107] O. K. Zahid, F. Wang, J. A. Ruzicka, E. W. Taylor, A. R. Hall, *Nano Lett.* **2016**, *16*, 2033.

[108] J. D. Uram, K. Ke, M. Mayer, *ACS Nano* **2008**, *2*, 857.

[109] V. Dimitrov, U. Mirsaidov, D. Wang, T. Sorsch, W. Mansfield, J. Miner, F. Klemens, R. Cirelli, S. Yemenicioglu, G. Timp, *Nanotechnology* **2010**, *21*, 065502.

[110] R. M. Smeets, N. H. Dekker, C. Dekker, *Nanotechnology* **2009**, *20*, 095501.

[111] R. M. Smeets, U. F. Keyser, N. H. Dekker, C. Dekker, *Proc. Natl. Acad. Sci. USA* **2008**, *105*, 417.

[112] D. P. Hoogerheide, S. Garaj, J. A. Golovchenko, *Phys. Rev. Lett.* **2009**, *102*, 256804.

[113] R. M. Smeets, U. F. Keyser, M. Y. Wu, N. H. Dekker, C. Dekker, *Phys. Rev. Lett.* **2006**, *97*, 088101.

[114] A. Radenovic, E. Trepagnier, R. Csencsits, K. H. Downing, J. Liphardt, *Appl. Phys. Lett.* **2008**, *93*, 183101.

[115] E. Beamish, H. Kwok, V. Tabard-Cossa, M. Godin, *Nanotechnology* **2012**, *23*, 405301.

[116] B. M. Venkatesan, A. B. Shah, J. M. Zuo, R. Bashir, *Adv. Funct. Mater.* **2010**, *20*, 1266.

[117] B. M. Venkatesan, D. Estrada, S. Banerjee, X. Jin, V. E. Dorgan, M. H. Bae, N. R. Aluru, E. Pop, R. Bashir, *ACS Nano* **2012**, *6*, 441.

[118] S. J. Heerema, G. F. Schneider, M. Rozemuller, L. Vicarelli, H. W. Zandbergen, C. Dekker, *Nanotechnology* **2015**, *26*, 074001.

[119] S. Garaj, S. Liu, J. A. Golovchenko, D. Branton, *Proc. Natl. Acad. Sci. USA* **2013**, *110*, 12192.

[120] M. C. Lim, M. H. Lee, K. B. Kim, T. J. Jeon, Y. R. Kim, *J. Nanosci. Nanotechnol.* **2015**, *15*, 5971.

[121] M.-H. Lee, J.-H. Lee, H.-M. Kim, Y.-R. Kim, T.-J. Jeon, Y. Eugene Pak, K.-B. Kim, *Microfluid. Nanofluid.* **2013**, *16*, 123.

[122] R. D. Bulushev, S. Marion, E. Petrova, S. J. Davis, S. J. Maerkl, A. Radenovic, *Nano Lett.* **2016**, *16*, 7882.

[123] P. B. Tiwari, L. Astudillo, J. Miksovska, X. Wang, W. Li, Y. Darici, J. He, *Nanoscale* **2014**, *6*, 10255.

[124] P. Nuttall, K. Lee, P. Ciccarella, M. Carminati, G. Ferrari, K. B. Kim, T. Albrecht, *J. Phys. Chem. B* **2016**, *120*, 2106.

[125] J. A. Rodriguez-Manzo, M. Puster, A. Nicolai, V. Meunier, M. Drndic, *ACS Nano* **2015**, *9*, 6555.

[126] I. Yanagi, T. Ishida, K. Fujisaki, K. Takeda, *Sci. Rep.* **2015**, *5*, 14656.

[127] B. M. Venkatesan, B. Dorvel, S. Yemenicioglu, N. Watkins, I. Petrov, R. Bashir, *Adv. Mater.* **2009**, *21*, 2771.

[128] J. Shim, J. A. Rivera, R. Bashir, *Nanoscale* **2013**, *5*, 10887.

[129] a) S. J. Heerema, C. Dekker, *Nat. Nanotechnol.* **2016**, *11*, 127; b) H. Arjmandi-Tash, L. A. Belyaeva, G. F. Schneider, *Chem. Soc. Rev.* **2016**, *45*, 476.

[130] J. Feng, M. Graf, K. Liu, D. Ovchinnikov, D. Dumcenco, M. Heiranian, V. Nandigana, N. R. Aluru, A. Kis, A. Radenovic, *Nature* **2016**, *536*, 197.

[131] a) A. G. Vieira, C. Luz-Lima, G. S. Pinheiro, Z. Lin, J. A. Rodriguez-Manzo, N. Perea-Lopez, A. L. Elias, M. Drndic, M. Terrones, H. Terrones, B. C. Viana, *Vib. Spectrosc.* **2016**, *86*, 270; b) G. Danda, P. Masih Das, Y. C. Chou, J. T. Mlack, W. M. Parkin, C. H. Naylor, K. Fujisawa, T. Zhang, L. B. Fulton, M. Terrones, A. T. Johnson, M. Drndic, *ACS Nano* **2017**, *11*, 1937.

[132] P. Waduge, J. Larkin, M. Upmanyu, S. Kar, M. Wanunu, *Small* **2015**, *11*, 597.

[133] B. N. Anderson, M. Muthukumar, A. Meller, *ACS Nano* **2013**, *7*, 1408.

[134] D. Wang, S. Harrer, B. Luan, G. Stolovitzky, H. Peng, A. Afzali-Ardakani, *Sci. Rep.* **2014**, *4*, 3985.

[135] E. C. Yusko, J. M. Johnson, S. Majd, P. Prangkio, R. C. Rollings, J. L. Li, J. Yang, M. Mayer, *Nat. Nanotechnol.* **2011**, *6*, 253.

[136] S. W. Kowalczyk, L. Kapinos, T. R. Blosser, T. Magalhaes, P. van Nies, R. Y. Lim, C. Dekker, *Nat. Nanotechnol.* **2011**, *6*, 433.

[137] Y. Liebes-Peer, H. Rapaport, N. Ashkenasy, *ACS Nano* **2014**, *8*, 6822.

[138] R. Wei, V. Gatterdam, R. Wieneke, R. Tampe, U. Rant, *Nat. Nanotechnol.* **2012**, *7*, 257.

[139] M. Wanunu, A. Meller, *Nano Lett.* **2007**, *7*, 1580.
[140] E. C. Yusko, P. Prangkio, D. Sept, R. C. Rollings, J. L. Li, M. Mayer, *ACS Nano* **2012**, *6*, 5909.
[141] S. Hernandez-Ainsa, U. F. Keyser, *Nanoscale* **2014**, *6*, 14121.
[142] A. R. Hall, A. Scott, D. Rotem, K. K. Mehta, H. Bayley, C. Dekker, *Nat. Nanotechnol.* **2010**, *5*, 874.
[143] N. A. Bell, C. R. Engst, M. Ablay, G. Divitini, C. Ducati, T. Liedl, U. F. Keyser, *Nano Lett.* **2012**, *12*, 512.
[144] R. Wei, T. G. Martin, U. Rant, H. Dietz, *Angew. Chem. Int. Ed.* **2012**, *51*, 4864.
[145] S. Hernandez-Ainsa, N. A. Bell, V. V. Thacker, K. Gopfrich, K. Misiunas, M. E. Fuentes-Perez, F. Moreno-Herrero, U. F. Keyser, *ACS Nano* **2013**, *7*, 6024.
[146] C. Plesa, A. N. Ananth, V. Linko, C. Gulcher, A. J. Katan, H. Dietz, C. Dekker, *ACS Nano* **2014**, *8*, 35.
[147] a) H. Chang, F. Kosari, G. Andreadakis, M. A. Alam, G. Vasmatzis, R. Bashir, *Nano Lett.* **2004**, *4*, 1551; b) R. M. Smeets, U. F. Keyser, D. Krapf, M. Y. Wu, N. H. Dekker, C. Dekker, *Nano Lett.* **2006**, *6*, 89.
[148] S. W. Kowalczyk, A. R. Hall, C. Dekker, *Nano Lett.* **2010**, *10*, 324.
[149] a) A. R. Hall, S. van Dorp, S. G. Lemay, C. Dekker, *Nano Lett.* **2009**, *9*, 4441; b) R. M. Smeets, S. W. Kowalczyk, A. R. Hall, N. H. Dekker, C. Dekker, *Nano Lett.* **2009**, *9*, 3089.
[150] A. Singer, S. Rapireddy, D. H. Ly, A. Meller, *Nano Lett.* **2012**, *12*, 1722.
[151] A. Singer, M. Wanunu, W. Morrison, H. Kuhn, M. Frank-Kamenetskii, A. Meller, *Nano Lett.* **2010**, *10*, 738.
[152] J. Shim, Y. Kim, G. I. Humphreys, A. M. Nardulli, F. Kosari, G. Vasmatzis, W. R. Taylor, D. A. Ahlquist, S. Myong, R. Bashir, *ACS Nano* **2015**, *9*, 290.
[153] C. Plesa, J. W. Ruitenberg, M. J. Witteveen, C. Dekker, *Nano Lett.* **2015**, *15*, 3153.
[154] S. Carson, S. T. Wick, P. A. Carr, M. Wanunu, C. A. Aguilar, *ACS Nano* **2015**, *9*, 12417.
[155] a) D. Japrung, A. Bahrami, A. Nadzeyka, L. Peto, S. Bauerdick, J. B. Edel, T. Albrecht, *J. Phys. Chem. B* **2014**, *118*, 11605; b) M. M. Marshall, J. Ruzicka, O. K. Zahid, V. C. Henrich, E. W. Taylor, A. R. Hall, *Langmuir* **2015**, *31*, 4582.
[156] C. Plesa, N. van Loo, P. Ketterer, H. Dietz, C. Dekker, *Nano Lett.* **2015**, *15*, 732.
[157] A. T. Carlsen, O. K. Zahid, J. A. Ruzicka, E. W. Taylor, A. R. Hall, *Nano Lett.* **2014**, *14*, 5488.
[158] M. Firnkes, D. Pedone, J. Knezevic, M. Doblinger, U. Rant, *Nano Lett.* **2010**, *10*, 2162.
[159] D. Fologea, B. Ledden, D. S. McNabb, J. Li, *Appl. Phys. Lett.* **2007**, *91*, 539011.
[160] A. P. Han, G. Schurmann, G. Mondin, R. A. Bitterli, N. G. Hegelbach, N. F. de Rooij, U. Staufer, *Appl. Phys. Lett.* **2006**, *88*, 3901.
[161] a) S. K. Kannam, S. C. Kim, P. R. Rogers, N. Gunn, J. Wagner, S. Harrer, M. T. Downton, *Nanotechnology* **2014**, *25*, 155502; b) L. Z. Wu, H. Liu, W. Y. Zhao, L. Wang, C. R. Hou, Q. J. Liu, Z. H. Lu, *Nanoscale Res. Lett.* **2014**, *9*, 1.
[162] C. Plesa, S. W. Kowalczyk, R. Zinsmeester, A. Y. Grosberg, Y. Rabin, C. Dekker, *Nano Lett.* **2013**, *13*, 658.
[163] S. J. Singer, P. A. Maher, M. P. Yaffe, *Proc. Natl. Acad. Sci. USA* **1987**, *84*, 1015.
[164] a) K. J. Freedman, S. R. Haq, J. B. Edel, P. Jemth, M. J. Kim, *Sci. Rep.* **2013**, *3*, 1638; b) K. J. Freedman, M. Jurgens, A. Prabhu, C. W. Ahn, P. Jemth, J. B. Edel, M. J. Kim, *Anal. Chem.* **2011**, *83*, 5137; c) A. Oukhaled, B. Cressiot, L. Bacri, M. Pastoriza-Gallego, J. M. Betton, E. Bourhis, R. Jede, J. Gierak, L. Auvray, J. Pelta, *ACS Nano* **2011**, *5*, 3628; d) B. Cressiot, A. Oukhaled, G. Patriarche, M. Pastoriza-Gallego, J. M. Betton, L. Auvray, M. Muthukumar, L. Bacri, J. Pelta, *ACS Nano* **2012**, *6*, 6236; e) D. Japrung, J. Dogan, K. Freedman, A. Nadzeyka, S. Bauerdick, T. Albrecht, M. J. Kim, P. Jemth, J. B. Edel, *Anal. Chem.* **2013**, *85*, 2449; f) N. Martyushenko, N. A. Bell, R. D. Lamboll, U. F. Keyser, *Analyst* **2015**, *140*, 4882; g) R. Hu, J. Diao, J. Li, Z. Tang, X. Li, J. Leitz, J. Long, J. Liu, D. Yu, Q. Zhao, *Sci. Rep.* **2016**, *6*, 20776; h) E. C. Yusko, B. R. Bruhn, O. M. Eggenberger, J. Houghtaling, R. C. Rollings, N. C. Walsh, S. Nandivada, M. Pindrus, A. R. Hall, D. Sept, J. Li, D. S. Kalonia, M. Mayer, *Nat. Nanotechnol.* **2017**, *12*, 360.
[165] D. Y. Ling, X. S. Ling, *J. Phys.: Condens. Matter* **2013**, *25*, 375102.
[166] L. Restrepo-Perez, S. John, A. Aksimentiev, C. Joo, C. Dekker, *Nanoscale* **2017**, *9*, 11685.
[167] P. Waduge, R. Hu, P. Bandarkar, H. Yamazaki, B. Cressiot, Q. Zhao, P. C. Whitford, M. Wanunu, *ACS Nano* **2017**, *11*, 5706.
[168] J. D. Uram, K. Ke, A. J. Hunt, M. Mayer, *Small* **2006**, *2*, 967.
[169] a) J. D. Uram, K. Ke, A. J. Hunt, M. Mayer, *Angew. Chem., Int. Ed. Engl.* **2006**, *45*, 2281; b) A. Han, M. Creus, G. Schürmann, V. Linder, T. R. Ward, N. F. de Rooij, U. Staufer, *Anal. Chem.* **2008**, *80*, 4651; c) T. Takakura, I. Yanagi, Y. Goto, Y. Ishige, Y. Kohara, *Appl. Phys. Lett.* **2016**, *108*, 123701.
[170] P. H. Kussie, S. Gorina, V. Marechal, B. Elenbaas, J. Moreau, A. J. Levine, N. P. Pavletich, *Science* **1996**, *274*, 948.